JNeurosci
THE JOURNAL OF NEUROSCIENCE

***Research Report: Regular Manuscript***

# PDK1 regulates the maintenance of cell body and the development of dendrites of purkinje cells by pS6 and PKCγ

https://doi.org/10.1523/JNEUROSCI.2496-19.2020

**Cite as:** J. Neurosci 2020; 10.1523/JNEUROSCI.2496-19.2020

Received: 18 October 2019
Revised: 20 May 2020
Accepted: 21 May 2020

# PDK1 regulates the maintenance of cell body and the development of dendrites of purkinje cells by pS6 and PKCγ

Rui Liu[1†], Min Xu[1 †], Xiao-Yang Zhang[3], Min-Jie Zhou[1], Bing-Yao Zhou[1], Cui Qi[1], Bo Song[3], Qi Fan[1], Wei-Yan You[1], Jing-Ning Zhu[3], Zhong-Zhou Yang[4], Jun Gao[1,2*]

*1. Department of Neurobiology, Key Laboratory of Human Functional Genomics of Jiangsu, Nanjing Medical University, Nanjing, Jiangsu 211166, China.*

*2. Department of Rehabilitation Medicine, Jiangsu Shengze Hospital Affiliated to Nanjing Medical University, Suzhou, Jiangsu 215228, China.*

*3. Department of Biological Science and Technology and State Key Laboratory of Pharmaceutical Biotechnology, School of Life Sciences, Nanjing University, Nanjing, China.*

*4. State Key Laboratory of Pharmaceutical Biotechnology, Department of Cardiology, Nanjing Drum Tower Hospital, The Affiliated Hospital of Nanjing University Medical School and MOE Key Laboratory of Model Animal for Disease Study, Model Animal Research Center, Nanjing University, Nanjing 210061, China*

[†] These authors contributed equally to this work.

***Authors for correspondence: Dr. Jun Gao**

Jun Gao, Ph.D.

Professor and Dean of Department of Neurobiology,

School of Basic Medical Sciences,

Nanjing Medical University,

Longmian Road 101, Jiangning District,

Nanjing, Jiangsu, 211166, P. R. China.

Email: gaojun@njmu.edu.cn

Tel: 86-025-86869347

**Author contributions**

JG conceived the study; JG and RL designed the research; RL performed the immunostaining, mice intraperitoneal injection, 2D - reconstruction of PCs dendrites

and analysed the data; MX performed the genotyping and the western blotting; RL and MX performed the behavioural testing; ZX, SB and ZJ performed the whole-cell patch clamp recordings; CQ and MZ contributed to animal care; RL and BZ performed the Golgi staining and rAAV virus injections; BZ, MX, QF and WY performed the statistical analyses; ZY maintained the *Pdk1*$^{fl/fl}$ mouse line; and RL and JG wrote the paper.

**Number of Pages**: 38

**Number of Figures**: 12

**Number of Tables**: 6

**Number of Movies**: 2

**Number of words:** Abstract 225, Introduction 628, Discussion 1500

**Declaration of Interests**

The authors declare that they have no competing financial interests.

**Acknowledgements**

This work was financially supported by grants from the Natural Science Foundation of Jiangsu Province, China (Grants No. BK20171063) and the China Postdoctoral Science Foundation (Grants No. 2018M632336) to R.L. and the National Natural Science Foundation of China (Grants No. 81973308 and 81673416) and the Key R&D Program of Jiangsu Province (Grants No. BE2016761 and 2017CX010) to J.G. We thank Dr. Dario Alessi for providing the *Pdk1*$^{fl/fl}$ mice, Prof. Li - Huei Tsai for providing the *PV-cre* mice and Prof. Ying Shen for providing the *Pcp2-cre* mice. We also thank Prof. Ying Shen for technical advice and helpful discussions.

**Abstract**

3-Phosphoinositide-dependent protein kinase-1 (PDK1) plays a critical role in the development of mammalian brain. Here, we investigated the role of PDK1 in purkinje cells (PCs) by generating the PDK1 conditional knockout mice (PDK1-cKO) through crossing *PV-cre* or *Pcp2-cre* mice with *Pdk1*$^{fl/fl}$ mice. The male mice were used in the behavioural testing and the other experiments were performed on mice of both genders. These PDK1-cKO mice displayed the decreased cerebellar size and the impaired motor balance and coordination. By the electrophysiological recording, we observed the reduced spontaneous firing of PCs from the cerebellar slices of the PDK1-cKO mice. Moreover, the cell body size of PCs in the PDK1-cKO mice was time-dependently reduced compared to that in the control mice. And the morphological complexity of PCs was also decreased after PDK1 deletion. These effects may be contributed to the reduction of the rpS6 phosphorylation and the PKCγ expression in PDK1-cKO mice since the upregulation of pS6 by the treatment of 3BDO, the agonist of mTOR1, partly rescued the reduction in the cell body size of the PCs, and the delivery of rAAV-PKCγ through cerebellar injection rescued the reduced complexity of the dendritic arbour inPDK1-cKO mice. Taken together, our data suggest that PDK1, by regulating rpS6 phosphorylation and PKCγ expression, controls the cell body maintenance and the dendritic development in PCs and is critical for cerebellar motor coordination.

**Key words:** PDK1, cerebellum, purkinje cells, pS6, PKCγ, cell body

**Significance Statement:**

Here, we show the role of PDK1 in PCs. The ablation of PDK1 in PCs resulted in a reduction of the cell body size, and the dendritic complexity and the abnormal spontaneous firing, which attributes to the motor defects in PDK1-cKO mice. Moreover, the rpS6 phosphorylation and the expression of PKCγ are down-regulated after the ablation of PDK1. Additionally, upregulation of rpS6 phosphorylation by 3BDO partly rescued the reduction in cell body size of PCs, and overexpression of

PKCγ in PDK1-KO PCs rescued the reduction in the dendritic complexity. These findings indicate that PDK1 contributes to the maintenance of cell body and the dendritic development of PCs by regulating rpS6 phosphorylation and PKCγ expression.

## Introduction

Purkinje cells (PCs) are the sole output neuron of the cerebellar cortex, serving as an integration centre in this region, and are important for motor coordination and motor balance (Lui et al., 2017; Edamakanti et al., 2018; Popa et al., 2019). Although the neurogenesis and neuronal migration of PCs are completed during the embryonic stage, the postnatal development process is critical for PCs and cerebellum-related motor function (Liu et al., 2017; Lui et al., 2017; Edamakanti et al., 2018). During the 8-week postnatal stage, the soma size of PCs gradually increases and the characteristic dendritic trees of PCs are also formed at this stage (Takeo et al., 2015). Previous studies have demonstrated that mTOR (the mammalian target of rapamycin) pathway may be involved in the postnatal development of PCs. For example, in PC-specific deletion of mTORC1 mice, PCs are progressively lost due to apoptosis that is paralleled by the age-dependent motor deficits (Angliker et al., 2015). Moreover, the whole-brain mTORC2 knockout mice display the motor coordination defects, which correlates with the reduced Purkinje cell body size, the developmental deficits in climbing fibre elimination and the impaired dendritic self-avoidance. Furthermore, the deletion mTORC2 in cerebellum leads to a striking decrease in the activation and expression of several protein kinase C (PKC) isoforms including the gamma isoform of PKC (PKCγ) (Thomanetz et al., 2013; Angliker et al., 2015). Previous studies have reported that PKCγ, which is highly and specifically expressed in PCs, plays a critical role in the eliminating supernumerary climbing fibre synapses form developing PCs (Kano et al., 1995; Hirai, 2018). Although various molecules and mechanisms have been implicated in the regulation of PC morphogenesis, the mechanisms that regulate postnatal maintenance and development of PCs remain unclear.

The 3-phosphoinositide-dependent protein kinase-1 (PDK1), a serine/threonine kinase of the AGC kinase group, phosphorylates and activates at least 23 other AGC protein kinases such as AKT (Protein Kinase B), PKC, ribosomal protein S6 kinase B1 (S6K1) and serum- and glucocorticoid-induced kinase (SGK) (Castel et al., 2016; Leroux et al., 2018) which contributes to many biological processes, including cell polarization, neuronal migration, and neuronal differentiation (Oishi et al., 2009; Dainichi et al., 2016; Itoh et al., 2016; Wang et al., 2017b). Our previous studies showed that PDK1 is required for the proliferation, differentiation, and migration of neural progenitor cells (NPCs) during dentate gyrus (DG) development (Xu et al., 2019). Whole-brain downregulation of PDK1-AKT signalling results in microcephaly, reflected in a reduction in cell size rather than cell number (Lawlor et al., 2002; Cordon-Barris et al., 2016). Additionally, PDK1 is a downstream antagonist of phosphatase and tensin homologue (PTEN), and the hypertrophy of PTEN-deficient neuronal nuclei and soma can be rescued by the PDK1 deletion (Chalhoub et al., 2009; Grego-Bessa et al., 2016). Recent evidence indicates that the loss of PTEN in PCs results in autistic-like traits, including motor learning deficits, sociability impairment, and repetitive behaviour, which may be attributed to the structural abnormalities in neurite and the late-onset cell death (Cupolillo et al., 2016). These data indicate that PDK1 is likely involved in the postnatal development of PCs.

In this study, we investigated the role of PDK1 in the postnatal development of PCs by crossing the *Pdk1*$^{fl/fl}$ mice with the *PV-cre* or *Pcp2-cre* line. And our data showed that the ablation of PDK1 in PCs decreased the cell body size, reduced the dendritic complexity, and was associated with substantial abnormal spontaneous electrophysiological properties in PCs, which was paralleled by the motor defects. We further showed that the reduced ribosomal protein S6 (rpS6) phosphorylation and expression of PKCγ was probably contributed to these phenotypes. Together, our results suggested that PDK1 was important for the cell body maintenance and the dendritic development in postnatal PCs and was correlated to the cerebellar motor coordination and balance.

## Materials and Methods

### Animals and mouse breeding

*Pdk1*$^{fl/fl}$ mice have been reported previously (Lawlor et al., 2002). *Parvalbumin-cre* (*PV-cre*) mice were generously provided by Prof. Li - Huei Tsai (Picower Institute for Learning and Memory, MIT, MA, USA). *Pcp2-cre* mice were generously provided by Prof. Ying Shen (Zhejiang University, Hangzhou, Zhejiang, PRC) (Barski et al., 2000). *ROSA26-LSL-EYFP* mice were generously provided by Prof. Chunjie Zhao (Southeast University, Nanjing, Jiangsu, PRC) (Srinivas et al., 2001). The *PV-cre*; *Pdk1*$^{fl/fl}$ mice and the *Pcp2-cre*; *Pdk1*$^{fl/fl}$ mice were generated by crossing the *Pdk1*$^{fl/fl}$ mice with the *PV-cre* mice and the *Pcp2-cre*; *Pdk1*$^{fl/fl}$ mice respectively. In this study, the *PV-cre*; *Pdk1*$^{fl/fl}$ mice and the *Pcp2-cre*; *Pdk1*$^{fl/fl}$ mice were named cKO-PV and cKO-Pcp2 respectively, and the *Pdk1*$^{fl/fl}$ mice were grouped as control (Ctrl). All the mice are maintained on a C57/B6 background and kept in a barrier facility, and all animal experiments were conducted in accordance with the procedure approved by the Animal Ethical and Welfare Committee for Institutional Animal Care and Use Committee (IACUC) of Nanjing Medical University (Approval No. IACUC-1907019). The day of birth was considered as postnatal day 0 (P0).

### Tissue collection

Mice (P14 - P120) were anesthetized by intraperitoneal administration of ketamine/xylazine (ketamine: 100 mg/kg; xylazine: 10 mg/kg) based on body weight and sacrificed by transcardial perfusion with phosphate-buffered saline (PBS) followed by 4% paraformaldehyde (PFA) in PBS. The cerebellum was removed and post-fixed in 4% PFA overnight at 4°C and processed into cryosections by using a freezing microtome (Leica, CM 1950, 25 μm thick).

### Genotyping

Genotype was identified by PCR with genomic DNA obtained from the toes or the tails. The primers sequences used to identify specific genotypes were as follows: *Pdk1*$^{fl/fl}$ 5’-CTATGCTGTGTTACTTCTTGGAGCACAG-3’ and

5'-TGTGGACAAACAGCAATGAACATACACGC-3'; *Pcp2-cre* and *PV-cre* 5'-CATACCTGGAAAATGCTTCTGTCC-3' and 5'-TCCCCAGAAATGCCAGATTACG-3'; *ROSA26-LSL-EYFP* 5'-AAGACCGCGAAGAGTTTGTC-3' and 5'-AAAGTCGCTCTGAGTTGTTAT-3'. The PCR program used was; 94°C 5min, then 35 cycles of 94°C 30 seconds for denaturation, 62°C 45 seconds for annealing and 72°C 45 seconds for elongation.

**Behavioural Testing**

All behavioural experiments were conducted on male mice between 09:00 hours and 16:00 hours. Each mouse was subjected to each of the following behavioural tests.

**Footprint**

Hind paws and forepaws of mice were painted with nontoxic blue and red watercolour respectively. Mice walked through a tunnel (100 cm Long, 9 cm wide, 60 cm high) with white paper lining the floor to a dark box with a hole. Each mouse was trained on 3 consecutive days with 3 trials per day. Footprint patterns were analysed for length of stride, stance, and sway and distance between the front and hind footprints on each side. For each measurement, the first and last 20 cm of the prints were excluded. If the mouse stopped in the middle of the tunnel, the trial was repeated.

**Rotarod assay**

The rotarod apparatus (ZH-300) was used to measure motor coordination as previously described (Carter et al., 1999). During the training period, each mouse was placed on the rotarod at a constant speed (20 rpm) for a maximum of 60 seconds. Mice received six trials per day for 4 consecutive days, by which time a steady baseline level of performance was attained. Mice then received two trials at 6 independent speed levels: 10, 15, 20, 25, 30, and 33 rpm. The mean latency to fall off the rotarod (for the two trials at each speed level) was recorded and used in subsequent analysis.

**Elevated beam-walk assay**

The elevated beam-walk assay for evaluating motor balance was carried out as previously described (Carter et al., 2001). Briefly, the beams consisted of long strips

of matte-surface acrylic (130 cm) with a 28- or 12-mm square cross-section and a 30, 16, or 10 mm diameter. The beams were placed horizontally, 40 cm above the platform surface, with one end mounted on a narrow support and the other end attached to an enclosed box (30 cm square) into which the mouse could escape. In the middle part of each beam an 80-cm long segment was marked. One angle poise light (40 W) was positioned above and to one side of the start of the beam. During training, mice were placed at the start of the 12-mm square beam and encouraged to traverse it. Each mouse underwent 3 consecutive trials and was then returned to its home cage to rest for 30 minutes, then another 3 consecutive trials were performed. Each mouse underwent 6 trials per day over 4 days. On the $5^{th}$ day, each mouse underwent three consecutive trials on each of the round beams, from the widest to the narrowest beam. The latency to traverse each 80-cm section and the number of times the hind paws slipped off each beam were recorded for each trial. Mice were allowed up to 60s to cross the beam. If the mouse dropped from the beam, the trial was repeated, and if it could not cross the beam within 60s after 2 attempts, the trial was allocated a maximum latency of 60s for inclusion in the latency analyses. Analysis of each measure was based on the mean scores of the two trials for each beam.

**Immunofluorescence**

Immunofluorescence experiments were performed as previously described (Liu et al., 2015). Briefly, brain tissue sectioning was performed using a freezing microtome (Leica, CM 1950, 25 μm thick). For each genotype, at least three histological sections at middle sagittal levels from three different animals were analysed for immunostaining, and confocal optical sections were acquired. The primary antibodies and working concentration were as follows: rabbit anti-calbindin (Abcam, ab49899, 1 μg/mL), anti-NeuN (Millipore, ABN78, 1 μg/mL), anti-PAX6 (Abcam, ab5790, 4 μg/mL), anti-PDk1 (Epitomics, 3377-1, 2 μg/mL), anti-PDk1 (Abcam, ab52893, 0.36 μg/mL), anti-PKC (phospho T514) (Abcam, ab109539, 0.68 μg/mL), anti-Phospho-S6 Ribosomal Protein (Ser235/236) (Cell Signalling Technology, #2211, $3.8 \times 10^{-2}$ μg/mL); mouse anti-NeuN (Millipore, MAB377,2 μg/mL), anti-GFAP (Millipore,

MAB3402, 1 μg/mL), anti-GAD67 (Millipore, MAB5406, 1 μg/mL), anti-mCherry (Bioworld Technology Inc, Louis Park, MN, MB2013, 1 μg/mL); chicken anti-GFP (Abcam, ab13970, 2.5 μg/mL). The secondary antibodies included DyLight 488 donkey anti-rabbit (Thermo Fisher Scientific, SA5-10038, 1 μg/mL), Alexa Fluor 488 goat anti-rabbit (Invitrogen, A11008, 4 μg/mL), DyLight 488 donkey anti-mouse (Thermo Fisher Scientific, SA5-10166, 1 μg/mL), Alexa Fluor 555 donkey anti-rabbit (Invitrogen, A31572, 4 μg/mL), DyLight 550 donkey anti-mouse (Thermo Fisher Scientific, SA5-10167, 1 μg/mL), Alexa Fluor 488 donkey anti-chicken (Jackson ImmunoResearch Laboratories, INC, 703-545-155, 0.25 μg/mL). Secondary antibodies were diluted in PBS containing 10% Fetal Bovine Serum (FBS), 0.1% Triton X-100 and 0.5 μg/mL DAPI (4,6-diamidino-2-phenylindole).

**Golgi staining**

Golgi staining was performed using FD Rapid GolgiStain$^{TM}$ Kit (FD NeuroTechnologies, INC, #PK401) following the manufacturer's protocols. Briefly, the cerebellum was dissected from P30 mice and incubated in premixed Solutions A and B that were refreshed the next day. The cerebellum was kept in the dark for 2 weeks at room temperature, then incubated in Solution C in the dark for 5 - 7 days at room temperature. The cerebellum was then sectioned into 250 μm thick slices with a vibratome (VT1000; Leica Microsystems) and stained according to the manufacturer's protocols. Images of PCs and other cerebellar neurons were captured by Olympus Fluoview FV1200 confocal microscope.

The dendritic arbours of each PC was semi-autonomous traced by using NIH ImageJ software as previously described (Stanko et al., 2015). Dendritic arborization complexity was assessed using a Sholl analysis to examine dendritic intersections per 1 μm concentric radial interval from cell body (Ferreira et al., 2014). The schematic representation of the Sholl analysis method described is shown in Figure 12 G and H. The significance of the differences in complexity was determined using GraphPad Prism software with a two-way ANOVA (genotype and circle radius as factors) followed by the Bonferroni's *post hoc* test.

**Western blotting**

Western blotting experiments were performed as previously described (Xu et al., 2019). Briefly, mouse cerebellums were collected and homogenized and the lysates from at least four brains per genotype were clarified by centrifugation at 14000 rpm. The protein concentrations were measured (Pierce Biotechnology, Rockford, IL). Cerebellum lysates (20 μg) were separated by 10% SDS-PAGE and transferred to PVDF membranes. After blocking the membranes with 5% non-fat dry milk in Tris-buffered saline with 0.5% Tween-20, they were incubated at 4°C with primary antibodies, followed by incubation with the HRP-linked anti-rabbit IgG secondary antibody (Cell Signaling Technology, 7074, $8.2 \times 10^{-3}$ μg/mL), and signals detected using SuperSignal West Pico Chemiluminescent Substrate (Thermo Scientific). The primary antibodies used and the working concentration of these antibodies were: rabbit anti-β-actin (Bioworld Technology Inc, Louis Park, MN, AP0060, 1 μg/mL), anti-GAPDH (Cell Signaling Technology, 2118, $8.4 \times 10^{-3}$ μg/mL), anti-PDk1 (Epitomics, 3377-1, 0.5 μg/mL), anti-PDk1 (Abcam, ab52893, 0.09 μg/mL), and anti PKCγ (Abcam, ab4145, 0.1 μg/mL).

**Whole-cell patch clamp recordings on brain slices**

Whole-cell patch clamp recordings on brain slices were performed as previously described (Wang et al., 2017c). Briefly, cerebellar slices (300 μm in thickness) were prepared following the standard protocols. During whole-cell patch-clamp recordings, PCs were held at a membrane potential of -70 mV and characterized by injection of rectangular voltage pulse (5 mV, 50 ms) to monitor the whole-cell membrane capacitance, membrane resistance and series resistance. PCs were excluded from the experiments if the series resistance was not stable or exceeded 20 MΩ.

**3BDO treatment**

3-benzyl-5-((2-nitrophenoxy) methyl)-dihydrofuran-2(3H)-one (3BDO, Selleck chemicals, S8317) was dissolved in 100% DMSO and stored in a stock solution of

300 mg/mL at -20°C. A working solution was prepared immediately before injection at a final concentration of 6 mg/mL 3BDO, 2% DMSO, 0.01M PBS. P14 cKO-PV and *Pdk1*$^{fl/fl}$ mice were injected intraperitoneally with either 3BDO (80 mg/kg body weight/mouse) or vehicle once a day before harvest or behaviour test.

**Virus vector construction**

Total RNA extraction of the cerebellar cortices and cDNA synthesis were performed as previously described (Liu et al., 2015). Full-length PKCγ coding sequence was amplified from cDNA taken from a wild-type C57/B6 mouse and inserted into a pCAGIG plasmid (provided by Prof. Chunjie Zhao, Southeast University). Recombinant adeno-associated virus (AAVs) were produced by the Taiting Biological Co., Ltd (Shanghai, China) at the following stock titers (GC/mL): AAV2/9-CAG-FLEX-Prkcg-3xHA-P2A-EGFP at $6.7 \times 10^{12}$, AAV2/9-CAG-FLEX-EGFP at $2.3 \times 10^{13}$ and AAV2/8-CMV_bGI-mCherry at $2.77 \times 10^{13}$. Viruses were diluted in 0.01 mol/L sterile phosphate-buffered saline (PBS, pH = 7.4) before injection. The PCs in the Ctrl and cKO-Pcp2 mice was labeled using AAV2/8-CMV_bGI-mCherry constructs that express mCherry under a CMV promoter. Rescue experiments were conducted in *Pcp2-cre*; *Pdk1*$^{fl/fl}$ mice using rAAVs expressing enhanced green fluorescent protein (EGFP) or full-length PKCγ. rAAVs expressing EGFP under CAG promoters (AAV2/9-CAG-FLEX-EGFP) were used to label PDK1-KO PCs in mice, and rAAVs expressing both EGFP and PKCγ (AAV2/9-CAG-FLEX-Prkcg-3xHA-P2A-EGFP) were used to label PDK1-KO PCs and overexpress PKCγ. The PKCγ-expressing rAAV construct contained a CAG promoter and a floxed stop sequence upstream of an independent EGFP and full-length PKCγ sequence (rAAV2/9 - CAG - FLEX - Prkcg - 3xHA - P2A - EGFP). Thus, only Cre-positive PCs in the cKO-Pcp2 mice were able to remove the stop sequence and to overexpress EGFP and PKCγ. The rAAV2/9-CAG-FLEX-EGFP was used to express EGFP and to label Cre-positive PDK1-KO PCs in the cKO-Pcp2 mice without overexpression of PKCγ.

**Virus injections**

All injections were performed on newborn mouse pups at postnatal age P0 - P1 as previously described (Gibson and Ma, 2011). Briefly, the P0 or P1 mouse pubs were divided into two groups: one group were injected with a mix of AAV2/8-CMV_bGI-mCherry and AAV2/9-CAG-FLEX-EGFP in a 1:1 ratio, and the other group were were injected with a mix of AAV2/8-CMV_bGI-mCherry and AAV2/9-CAG-FLEX-Prkcg-3xHA-P2A-EGFP in a 1:1 ratio. Each pup was injected with 1 - 1.5 μL of diluted rAAVs, and the concentration is $1 \times 10^{12}$ GC/mL for each AAV vector so the final concentration is $1 \times 10^{12}$ GC/mL. A digital pressure pump and a Hamilton syringe with a beveled 34G stainless steel needle were used. Pups were then returned to their mothers and analysed at P30.

**Microscopic analysis**

The images were acquired on a Nikon (Tokyo, Japan) ECLIPSE Ti microscope or an Olympus FV1200 confocal microscope (Tokyo, Japan). All images were processed using Image-Pro Plus 6.0 software (Media Cybernetics), Adobe Photoshop CS6.0 software (Adobe Systems Inc, San Jose, CA), or the open source FIJI (NIH ImageJ) software (http://fiji.sc/Fiji).

**Analysis of PC dendrites**

Confocal z-stacks were collected on an Olympus FV1200 laser scanning confocal microscope (Tokyo, Japan). Confocal stacks of labelled PCs were collected from anatomical positions throughout the cerebellum. GFP-positive or mCherry-positive PC dendrites were manually traced to generate a skeletonized 2D reconstruction of the entire arbour as previously described (Stanko et al., 2015). Total dendrite area was calculated using the confocal stack images of each PC and total dendrite lengths were calculated from the 2D reconstruction. Dendritic arbour complexity was assessed using a Sholl analysis method, which was described in the methods for Golgi staining. All processes described above were performed using the open source FIJI (NIH ImageJ) software (http://fiji.sc/Fiji).

**Morphometric analysis**

The area of cerebellum, the thickness of ML of the cerebellum and the total number, the cell density and the cell body size of PCs were evaluated in the lobule II-III, V-VI and IX-X of cerebellum of Ctrl, cKO-PV and cKO-Pcp2 mice at different ages. Immunostaining of cerebellar slices with the specific antibody of calbindin was used to label the cell bodies and proximal primary dendrites of PCs, and a combination of immunostaining for calbindin and DAPI staining was used to label the outlines of sagittal cerebellar slices and to distinguish the three layers of the cerebellar cortex. The area of cerebellum was obtained by drawing the outline of sagittal sections of cerebellum and then calculating the average enclosed area. The size of each purkinje cell body was obtained by drawing the outline of PC body clearly showing a proximal primary dendrite. The total number of PCs was obtained by drawing the outline of purkinje cell layer (PCL) in the selected lobules of cerebellum and counting the number of PCs in the lobule manually. The length of the PCL was then measured and the density of PCs was calculated by dividing the total number of PCs by the length of PCL. At least six slices/mice and three mice (excepted for vehicle-treated cKO-PV mice) at each age point were analysed for each condition in parallel experiments. And for the analysis of the cell body size of PCs, at least 32 PCs per mouse were analysed for each condition in parallel experiments. All processes described above were performed using the open source FIJI (NIH ImageJ) software (http://fiji.sc/Fiji).

**Experimental Design and Statistical Analysis**

The male mice were used in the behavioural testing, and in the other experiments, .no effects of ewe, fetus, or gender were observed. All the data were statistically analysed using GraphPad Prism software (version 8, GraphPad Software). The data are expressed as the mean ± s.e.m. The error bars represent the standard error of the mean. For morphometric analysis, western blotting, electrophysiological analysis and behaviour tests, two-tailed unpaired Student's *t*-test, one-way ANOVA followed by the Bonferroni's *post hoc* test or two-way ANOVA followed by the Bonferroni's *post*

*hoc* test were used to analyse statistical significance. The statistical methods used in each experiment are described in the figure legends and the detailed description for each statistical test, including the degrees of freedom and the sample size, are shown in the figure legends or tables. If the P-values are less than 0.0001 or more than 0.9999, they were presented as $p < 0.0001$ or $p > 0.9999$ respectively. And in the other cases, the exact P-values are presented in the figure legends or tables. In the figures, P-values are presented as: ns, $p \geq 0.05$; * or # $p < 0.05$; ** or ## $p < 0.01$; and *** or ### $p < 0.001$.

## Results

### Cerebellar size was decreased in cKO-PV mice

Previous data demonstrated that Cre expression was evident in PCs no later than postnatal day 8 in *PV-cre* mice (Buttermore et al., 2012). To confirm the specificity of the *PV-cre* drivers, we generated *PV-cre*; *ROSA26-LSL-EYFP* mice and observed yellow fluorescent protein (YFP)-positive cells located in the molecular layer (ML) and PCL of cerebellum (Fig. 1A), suggesting that parvalbumin is expressed in PCs and ML interneurons in the cerebellar cortex. Co-immunostaining for YFP and the PC marker calbindin further confirmed that YFP was expressed in PCs (Fig. 1A - D). Furthermore, our data demonstrated that PDK1 is highly expressed in postnatal PCs (Fig. 1E - J''). To better understand the role of PDK1 in the postnatal development of PCs and motor dysfunction, we deleted *Pdk1* by crossing the $Pdk1^{fl/fl}$ mice with the *PV-cre* line. Immunostaining for PDK1 and glutamic acid decarboxylase 67 (GAD67), which is expressed in the cell bodies, dendrites, and axonal projections of PCs, showed a dramatic reduction in PDK1 abundance in PCs at P21, P40 and P60 in cKO-PV mice (Fig. 2A - F''), and the disruption efficiency was confirmed by western blot at P60 (Fig. 2G) (Nam et al., 2019). Moreover, our data indicated that PDK1-positive cells was detected in the granule cell layer (GCL) and the ML of cerebellum in the Ctrl mice at P60, and in the cKO-PV mice, PDK1-positive cells was detected in the GL of cerebellum but not in the ML of cerebellum (Fig. 2E - F''). We found that nearly all cKO-PV mice survived to adulthood. Moreover, the cerebellar

size was dramatically reduced, while the body weight, the brain weight and the brain architecture of the forebrain or midbrain in adult cKO-PV mice were similar to those in the Ctrl mice (Fig. 3A - D and Table 1). By immunostaining for PC marker calbindin, we observed that the sagittal cross-sectional area of the cerebellar vermis was decreased significantly beginning at P21 after the PDK1 deletion during the postnatal developmental stage, while the PCs density, the overall cytoarchitecture and foliation of the cerebellum were not changed in cKO-PV compared to those in Ctrl mice at P14, P21, P30 and P60 (Fig. 3E - J and Table 2). Moreover, the total numbers of PCs in cerebellar lobule V and VI from the Ctrl and cKO-PV mice were counted, and no significant differences were observed at P60, however, both the density and the total number of PCs was decreased at P120 in cKO-PV mice (Fig. 3J - L and Table 2). Moreover, to assess whether other types of cells were affected, the immunostaining for NeuN and GFAP, which are expressed in the cerebellar granule neurons and Bergmann glia respectively, were performed. As shown in Fig. 4, the distribution and cytoarchitecture of cerebellar granule neurons and the morphology of Bergmann glial fibres in the cKO-PV mice were similar to those in the Ctrl mice. Together, these data indicated that the deletion of PDK1 contributed to the reduction of cerebellar size in the cKO-PV mice.

**The cell body size and the morphological complexity of PCs were decreased in cKO-PV mice.**

To further study the morphology of PCs in the absence of PDK1, the cell body size of PCs was measured at P14, P21, P30 and P60. Compared to the Ctrl mice, the purkinje cell body size was time-dependently reduced, and the significant reduction was detected since P21 in cKO-PV mice (Fig. 5A - F and Table 2). As the cell body size of PCs was decreased in the cKO-PV mice, and the PC dendrites are located in the ML of the cerebellum, we next investigated whether the decreased cell body area after PDK1 ablation affected the cerebellar ML thickness at P14, P21, P30, P60 and P120. We observed that the ML thickness of cerebellar lobules V and VI was significantly increased at P21 in Ctrl mice compared to that at P14, while not in cKO-PV mice.

Moreover, the ML thickness of cerebellar lobules V was markedly decreased since P21, and the significant reduction of that in lobules VI was detected since P30 in the cKO-PV mice compared to that in the Ctrl mice (Fig. 5G - J' and Table 2). To confirm the presence of dysmorphic PC dendrites in the absence of PDK1, we used Golgi staining to examine the morphology of PCs from P30 mice and observed a severe decreased in the complexity of the dendritic arbour in cKO-PV mice compared to that in Ctrl (Fig. 5K - L). Thus, our data demonstrate that PDK1 is required for postnatal development and maintenance of PCs dendrites and suggest that the decreased cerebellum is due to the reduced ML thickness.

**The cKO-PV mice displayed motor defects.**

We observed that the cKO-PV mice staggered and demonstrated ataxia-like behaviour, indicating that PDK1 may be attributed to the proper motor control (Movie 1 and 2). To quantitatively analyse their gait defects, we performed a footprint assay at 9 - 10 weeks after birth of mice (Fig. 6A and A'). Moreover, a statistic analysis was performed by using the parameters illustrated in Fig. 6B. Our data demonstrated that the stride distance was similar in between the cKO-PV and the Ctrl mice; however, the stance lengths, the sway distance, and the overlap distance in the cKO-PV mice were significantly greater than those in the Ctrl mice (Fig. 6C - F and Table 3). These data indicated that PDK1 ablation resulted in wider gait and tottering steps in adult mice. We then performed an elevated beam-walk assay to examine whether the motor balance was affected after PDK1 deletion. A schematic diagram of an elevated beam-walk assay is shown in Fig. 6G. Most of the cKO-PV mice fell from the square beam (the side length: 28 mm) and could not finish the test at the age of 8 weeks (Fig. 6H). Furthermore, the rotarod test was used to investigate the effect the PDK1 ablation on the motor coordination. However, at the age of 8 weeks, no cKO-PV mice were able to stand on the rotating rod and to continue the test. These results indicated that the ablation of PDK1 leads to motor deficits at adult stage in cKO-PV mice.

To test whether the motor deficits observed in the adult cKO-PV mice were existed in developmental stage, the same behaviour tests were performed at 4 weeks after birth.

The cKO-PV mice took significantly longer time and showed more hind limb missteps to cross the beam with the diameters of 10 and 16 mm while not at 30 mm round beam test than the Ctrl mice did (Fig. 6I - J and Table 4). In rotarod assay, the cKO-PV mice fell off the rotarod in less time than the Ctrl mice did (Fig. 6K). Furthermore, we analysed the gait and observed no differences in the stance lengths, the sway distance, the overlap distance, or the stride distance between the cKO-PV mice and the Ctrl mice at 4 weeks after birth (Fig. 6L - O and Table 3). These results indicated that although the 4-week-old cKO-PV mice showed no significant gait abnormality, they displayed the altered motor coordination and motor balance. Together, our results suggest that the ablation of PDK1 in PCs and cerebellar ML interneurons leads to progressive motor deficits.

**PC-specific ablation of PDK1 resulted in decreased size of PCs and motor defects**

Because the *PV-cre* mice express Cre recombinase in all parvalbumin-positive interneurons in the nervous system, including PCs, basket cells (BCs) in the ML of cerebellum and a part of cerebral cortical GABAergic interneurons, we could not exclude the possibility that disrupted morphology of PCs and motor dysfunction in the cKO-PV mice were due to a deficient interaction between PCs and cerebellar ML interneurons or to the abnormal inhibitory signal from the cerebral cortical PV-positive GABAergic interneurons. To determine whether the effects of PDK1 on PCs were cell-autonomous or non-cell autonomous, Purkinje-cell protein 2 - cre (Pcp2-cre) mice were employed. Cre recombinase-dependent DNA recombination is evident in the PCs by P6 and fully established by 2 - 3 weeks in *Pcp2-cre* mice (Barski et al., 2000). As the cKO-PV mice, the expression of PDK1 was efficiently disrupted and the sagittal cross-sectional area of the cerebellar vermis was significantly decreased after PC-specific deletion of *Pdk1* in cKO-Pcp2 mice at P30 after birth (Fig. 7A - B'', Fig. 8A - E and Table 5). Further analysis showed that the cell body sizes of PCs in lobules II/III, V/VI and IX of the cerebellum was also decreased in the cKO-Pcp2 mice at P30 (Fig. 8 A' - B''', F and Table 5). Although comparable PC density was detected in the Ctrl mice and the cKO-Pcp2 mice, the ML

thicknesses were significantly reduced after PDK1 ablation at P30 (Fig. 8G, H and Table 5).

To further study whether specific deletion of PDK1 in PCs resulted in the same motor deficits as that in cKO-PV mice, the elevated beam-walk and rotarod assay were used. Consistent with the above results, the cKO-Pcp2 mice displayed the longer latency to traverse the 10 mm beams, a greater number of missteps and the shorter latency to fall off the rotarod than the Ctrl mice did at 9 weeks after birth (Fig. 8I - K and Table 6). However, the latency and number of missteps in cKO-Pcp2 mice were similar to those in Ctrl mice, when beams with diameters of 16 mm or 30 mm were used (Fig. 8I, J and Table 6), suggesting that the motor balance deficits are only detectable in the harder test in cKO-Pcp2 mice at the age of 9 weeks. Together, the results suggest that specific ablation of PDK1 in postnatal PCs leads to the decreased body size, the reduced cerebellar size and the motor deficits, indicating that the role of PDK1 in postnatal PC development is cell autonomous.

**Defects in spontaneous firing activity of PDK1-KO PCs**

To test whether the electrophysiological properties of PCs were affected by the absence of PDK1, we performed whole-cell patch-clamp recordings on PCs. To exclude the influence of the cerebellar ML on the PCs, the cerebellar slices were separated from cKO-Pcp2 mice at P21. From recordings of spontaneous PC firings, we observed that both of the PCs from the Ctrl and cKO-Pcp2 mice exhibited regular firing (Fig. 9A). We quantified the PC spontaneous firing patterns by testing the coefficient of variation (CV) of inter-spike intervals (ISIs) and observed no diffidence between PDK1-deficient and control PCs, however, the spontaneous firing frequency was remarkably lower in PDK1-KO PCs than that in control PCs (Fig. 9B - D). Furthermore, the membrane capacitance (Cm) of PDK1-KO PCs was decreased compared to that of the control cells (Fig. 9E), which might be due to the decreased cell body size of PCs after PDK1 ablation. Moreover, spontaneous excitatory postsynaptic currents (sEPSCs) were recorded and analysed to test the synaptic transmission to PCs with PDK1 knocked out (Fig. 9F). The amplitude and frequency

of sEPSCs recorded in PDK1-KO PCs were similar to those in control cells (Fig. 9G and H). Taken together, the ablation of PDK1 affected the electrophysiological properties of PCs at P21.

**The reduction of PC cell body size was partly rescued by treatment of 3BDO in Pdk1 cKO-PV mice.**

Previous studies have shown that downregulated catalytic activity of PDK1 causes decreased rpS6 phosphorylation (Zurashvili et al., 2013). Immunostaining for the phosphorylated form of rpS6 (pS6) was performed to measure the activation level of mTORC1. We performed co-immunostaining for pS6 and GAD67, which is expressed in the cell bodies, dendrites, and axonal projections of PCs, and observed that rpS6 phosphorylation was significantly lower in PCs at P14 in the cKO-PV mice than that in the Ctrl mice (Fig. 10A - B''). Furthermore, the staining for pS6 in PCs was completely disrupted at P21 after PDK1 deletion (Fig. 10C - D''). These results indicated that in PCs, PDK1 ablation decreased rpS6 phosphorylation.

To further test whether decreased rpS6 phosphorylation in cKO-PV mice results in decreased cell body size of PCs, 3-Benzyl-5-((2-nitrophenoxy) methyl)-dihydrofuran-2(3H)-one (3BDO), an activator of mTORC1, was used (Peng et al., 2014). The cKO-PV and Ctrl mice were treated daily with either 3BDO (80 mg/kg) or vehicle from P14 to P30, and the brains were harvested at P30. As shown in the Fig. 10E - H'', the reduced immunostaining intensity of pS6 in the PCs and Bergmann glia of cKO-PV mice was significantly increased by 3BDO treatments at P30. Moreover, the reduced cell body size of PCs in the cKO-PV mice was partly rescued after 3BDO treatment, although the PC body size was not as large as that in the Ctrl mice and 3BDO treatment did not affect the cell body size of control PCs (Fig. 10I - M). And this 3BDO treatment also partly rescued some behaviour deficits in cKO-PV mice. The latency to fall off the rotarod in the 3BDO-treated cKO-PV mice was similar to those in vehicle-treated Ctrl mice in the lower rotational speed range (≤ 20 rpm) while not in the high rotational speed range (≥ 25rpm) (Fig. 10N). These results suggest that when PDK1 is disrupted, decreased cerebellar mTORC1 activity

contributes, at least partially, to the reduction of cell body size of PCs and the motor coordination defects.

**The decreased dendritic complexity was partly rescued by PKCγ overexpression in Pdk1 cKO-Pcp2 mice.**

Moreover, PKCγ, a member of the PKC family of protein that is highly expressed in PCs, has been demonstrated to be involved in the impaired development of dendritic trees in cultured PKCγ-deficient PCs (Schrenk et al., 2002; Takahashi et al., 2017; Hirai, 2018). To investigate whether the expression or the phosphorylation level of PKCγ was affected and contributed to the dendritic deficits after PDK1 ablation in PCs, we performed immunostaining for phosphorylated form of PKCγ (pPKCγ). Although the immunostaining intensity for pPKCγ in PCs from cKO-PV mice was similar to that from Ctrl mice at P21, it was significantly decreased at P30 and P40 (Fig. 11A - C'). The co-immunostaining for pPKCγ and GAD67 further showed that the staining intensity for pPKCγ was completely disrupted in PCs after PDK1 deletion at P60 (Fig. 11D - E''). The western blot with the anti-total PKCγ protein showed that the expression level of total PKCγ protein from cerebellar lysate in cKO-PV mice was lower than that in Ctrl mice at P21 (Fig. 11F and F'). To test whether the reduction of PKCγ protein in PCs is specific, we performed the western blot with the anti-calbindin and found that the expression level of calbindin protein in the cerebellum is comparable in the Ctrl and cKO-PV mice (Fig. 11G and G'). Together, our data demonstrated that PDK1 ablation in PCs lead to a reduction in the expression of PKCγ.

To test the function of PKCγ in the dendritic defects of PDK1-KO PCs, we performed rescue experiments by injecting recombinant rAAV into the cerebellum of cKO-Pcp2 mice at P0 or P1 (Gibson and Ma, 2011). In this study, the Cre-positive PDK1-KO PCs in the cKO-Pcp2 mice infected by the rAAV-PKCγ-EGFP constructs were able to overexpress PKCγ and EGFP or express EGFP only. Meanwhile, the PCs in the Ctrl and the cKO-Pcp2 mice infected by mCherry - expressing rAAV construct were labelled by mCherry. Then we analysed the morphology of the PC dendrites at P30.

Our data showed that the complexity of dendritic arbours was significantly decreased in EGFP-positive PDK1-KO PCs compared to that in mCherry-positive control PCs (Fig. 12A - D and I). After the treatment of rAAV-PKCγ-EGFP, the complexity of dendritic arbours of PDK1-KO PCs was partly rescued (Fig. 12C - I). Furthermore, we observed that the PDK1 deletion in PCs decreased the cumulative length of the dendritic arbour and the dendritic tree area of PCs, which was also partly rescued by infection with rAAV-PKCγ-EGFP (Fig. 12A - H, J and K). Our data demonstrated that the abnormal dendritic arbours observed in PCs after PDK1 ablation were partly rescued by PKCγ overexpression, suggesting an important role for PKCγ in PC dendritic development.

## Discussion

In this study, we provided novel evidences for the role of PDK1 in the postnatal development of PCs and motor control. The deletion of PDK1 in PCs resulted in a decrease in the cell body size, the reduced dendritic complexity, abnormal spontaneous firing and motor defects. PDK1 was shown to regulate the rpS6 phosphorylation and the expression of PKCγ *in vivo*. Additionally, upregulation of pS6 in the cerebellar cortex partly rescued the reduction in cell body size, and overexpression of PKCγ in PDK1-KO PCs rescued the reduction in the dendritic complexity observed after PDK1 ablation. These findings reveal an essential role for PDK1 in the maintenance of cell body and postnatal dendritic development of PCs by regulating pS6 phosphorylation and PKCγ expression.

### PDK1 regulates cell body size and dendritic development in postnatal PCs.

In previous studies, downregulation of PDK1-AKT signalling led to a smaller brain size due to a reduction in neuronal cell size (Lawlor et al., 2002). Moreover, recent work showed that simultaneous haploinsufficiency of *Pdk1* and contiguous gene causes microcephaly, developmental delay, intellectual disability, and epilepsy (Mucha et al., 2019). In this study, we showed that the ablation of PDK1 in PCs and cerebellar ML interneurons using the *PV-cre* mouse line led to a reduction in cell body

size, associated with a reduction in dendritic complexity. Meanwhile, we used *Pcp2-cre* mice to specifically delete *Pdk1* in PCs and observed that the dendritic complexity was also decreased compared to those in the Ctrl mice. Because the dendrites of PCs are in the cerebellum ML, the decreased dendritic complexity and the cumulative length of the dendritic arbour are likely to lead to a decrease in cerebellar ML thickness and cerebellar size. Furthermore, in the cKO-Pcp2 mice, we observed similar deficits in morphology and motor skills to those observed in cKO-PV mice, which suggests that the role of PDK1 in regulating the maintenance of PC body size is cell autonomous.

Previous work has shown that downregulation of PDK1-AKT signalling is essential for neuronal survival; however, recent work suggests that PDK1 deficiency in the forebrain causes neuronal apoptosis during cerebral cortical development (Wang et al., 2017b; Xu et al., 2017; Xu et al., 2019). Our data demonstrate that the densities of PCs are not affected by *Pdk1* deletion before P60 but are decreased at P120. Taken together, our data indicate that PDK1 is indispensable for the survival of PCs during postnatal development before adulthood and is likely to have different roles during the ageing stage after adulthood.

**Specific inactivation of PDK1 in PCs results in deficits in motor balance, coordination and spontaneous firing.**

A previous study demonstrated that the observed effects of whole-brain PTEN loss on brain size and neuronal cell size are PDK1 dependent (Chalhoub et al., 2009). Recent work showed that the loss of PTEN in cerebellar PCs results in defects in spontaneous and evoked firing activity of PCs and autistic-like traits, including impaired sociability, repetitive behaviour, and deficits in motor learning (Cupolillo et al., 2016). Furthermore, PDK1 were upregulated significantly in patients with Parkinson's disease (PD) when compared with normal healthy controls, indicating PDK1 may be associated with the development of movement disorders (Wang et al., 2017a). In this study, decreased cell body size and dendritic complexity of PCs after PDK1 deletion suggest that Pdk1 deletion probably leads to deficits in motor control. Our data show

that cKO-PV mice show progressive gait abnormalities with deficient motor balance and coordination compared to Ctrl mice. Similar deficits in motor balance and coordination are observed in adult cKO-Pcp2 mice, in which *Pdk1* has been specifically disrupted in PCs. Together, these results demonstrate that PDK1 is required for the postnatal development of PC-related motor function in mice. Moreover, the deficits in motor balance and coordination are more severe in cKO-PV mice than those in cKO-Pcp2 mice. PDK1 are widely expressed in the entire brain including cerebellum, cerebral cortex and hippocampus (Yoshida et al., 1999). Previous studies proved that PDK1 is required for the generation of neocortical interneurons, and the neocortical PV-positive interneurons is required for motor coordination (Oishi et al., 2009; Xenos et al., 2018). Additionally, increased connectivity of BCs, PV-positive interneurons in the ML of cerebellum, are detected in human Spinocerebellar ataxia type 1 (SCA1) patients characterised by progressive loss of motor coordination (Edamakanti et al., 2018). In the cKO-PV mice, PDK1 is disrupted not only in PCs but also in the neocortical PV-positive interneurons and the BCs, but in the cKO-Pcp2 mice, PDK1 is only deleted in PCs in the cerebellum. Thus, a wider range of PDK1 deletion in the cKO-PV mice than that in the cKO-Pcp2 mice is likely to explain the more severe motor defects in the cKO-PV mice.

The motor defects and decrease in the cell body size of PCs after PDK1 ablation led us to hypothesize that the electrophysiological properties of PCs would also be affected. In PDK1-KO PCs, the spontaneous firing frequency and the membrane capacitance (Cm) are lower than those of control cells, probably due to the decreased cell body size of the PCs (Tolias et al., 2005). Our findings demonstrate a new role for PDK1 in the development of PC-related motor function and, taken together, greatly improve our overall understanding of the postnatal development of PCs.

**PDK1 regulates the postnatal maintenance of PCs by inducing rpS6 phosphorylation and PKCγ expression.**

Previous studies have shown that the PDK1-SGK1 (serum/glucocorticoid-regulated kinase 1) axis activates mTORC1 by phosphorylating and inhibiting tubercular

687 sclerosis complex 2 (TSC2), and the inactivation of mTORC1 in PCs leads to a
688 reduction in cell body size, dendritic degeneration, axonal swelling, and
689 age-dependent apoptosis (Angliker et al., 2015; Castel et al., 2016). We used the
690 phosphorylation state of rpS6 as a marker for the level of activation of the mTORC1
691 pathway in PCs. Our data show that the intensity of pS6 in PCs was disrupted
692 beginning at P14, suggesting that mTORC1 activation is disrupted after the ablation
693 of PDK1. Additionally, daily intraperitoneal injection of cKO-PV and Ctrl mice with
694 3BDO or vehicle was performed and our data showed that 3BDO treatment partly
695 rescued the reduction in PC cell body size in cKO-PV mice, indicating that PDK1
696 regulates the development of PC body size partly through mTORC1 activation.
697 Moreover, our data show that the motor coordination of the 3BDO-treated cKO-PV
698 mice is similar to those of the vehicle - treated Ctrl mice in the low rotational speed
699 range, but is disrupted in the high rotational speed. These data suggest that decreased
700 cerebellar mTORC1 possibly contributes to the motor coordination defects after the
701 ablation of PDK1.
702 There is fourfold greater expression of PKCγ in the cerebellum than the average
703 expression in the rest of the brain, and PKCγ is expressed solely in PCs in the
704 cerebellum (Takahashi et al., 2017). Previous studies have suggested that PKCγ plays
705 a pivotal role in climbing fibre pruning in developing PCs, and cultured PCs from
706 PKCγ-deficient mice show impaired dendritic trees (Kano et al., 1995; Schrenk et al.,
707 2002; Hirai, 2018). Increased constitutive activity of PKCγ may be one but not the
708 only cause of SCA14, a neurological disease characterized by motor dysfunction and
709 death of PCs (Takahashi et al., 2015; Shimobayashi and Kapfhammer, 2017;
710 Nakazono et al., 2018; Wong et al., 2018; Trzesniewski et al., 2019). In this study,
711 immunoblotting test with anti-PKCγ antibody demonstrates that the expression level
712 of PKCγ in cKO-PV mice is reduced to 66% compared to that in Ctrl mice at P21.
713 However, immunostaining with the anti-pPKCγ (phospho T514) antibody shows that
714 a significant reduction of phosphorylation level of PKCγ is first detected in cKO-PV
715 mice at P40. One possible explanation is that the remaining PKCγ in cKO-PV mice
716 can be detected by immunostaining of cerebellar frozen section, further studies are

717 needed to exclude other possibilities. Taken together, we show a progressive loss of
718 phosphorylation level of PKCγ in cKO-PV mice after P30, which is probably due to
719 reduction of PKCγ expression. we hypothesize that the deficient dendritic complexity
720 in PCs after PDK1 ablation is a consequence of the downregulation of PKCγ
721 expression. To test this hypothesis, we overexpressed PKCγ in PDK1-KO PCs by
722 injecting an rAAV construct into the cerebellum of cKO-Pcp2 mice at P0. Our data
723 showed that the dendritic size and complexity of the PKCγ-overexpressing PDK1-KO
724 PCs are increased significantly compared to those of the PDK1-KO PCs. Thus, our
725 data indicate that PDK1 regulates the dendritic development of PCs by PKCγ.
726 Recently, the RORα was reported to plays multiple roles in PC dendritic genesis,
727 dendrite regression and maintenance of mature dendrites, at specific time windows
728 during development and throughout adulthood (Chen et al., 2013; Takeo et al., 2015).
729 The possible role of RORα in the PDK1 cKO mice is needed our further studies.
730 In summary, our data show that PDK1 contributes to cell body maintenance and
731 dendritic development in postnatal PCs by rPS6 and PKCγ. Continued work exploring
732 the signalling pathway through which PDK1 regulates rPS6 phosphorylation and
733 PKCγ expression will facilitate understanding of PCs postnatal developmental
734 program and cerebellar motor coordination.
735
736 **References:**
737 Angliker N, Burri M, Zaichuk M, Fritschy JM, Ruegg MA (2015) mTORC1 and
738 mTORC2 have largely distinct functions in Purkinje cells. Eur J Neurosci
739 42:2595-2612.
740 Barski JJ, Dethleffsen K, Meyer M (2000) Cre recombinase expression in cerebellar
741 Purkinje cells. Genesis 28:93-98.
742 Buttermore ED, Piochon C, Wallace ML, Philpot BD, Hansel C, Bhat MA (2012)
743 Pinceau organization in the cerebellum requires distinct functions of neurofascin in
744 Purkinje and basket neurons during postnatal development. The Journal of
745 neuroscience : the official journal of the Society for Neuroscience 32:4724-4742.
746 Carter RJ, Morton J, Dunnett SB (2001) Motor coordination and balance in rodents.

747 Curr Protoc Neurosci Chapter 8:Unit 8 12.
748 Carter RJ, Lione LA, Humby T, Mangiarini L, Mahal A, Bates GP, Dunnett SB,
749 Morton AJ (1999) Characterization of progressive motor deficits in mice transgenic
750 for the human Huntington's disease mutation. The Journal of neuroscience : the
751 official journal of the Society for Neuroscience 19:3248-3257.
752 Castel P, Ellis H, Bago R, Toska E, Razavi P, Carmona FJ, Kannan S, Verma CS,
753 Dickler M, Chandarlapaty S, Brogi E, Alessi DR, Baselga J, Scaltriti M (2016)
754 PDK1-SGK1 Signaling Sustains AKT-Independent mTORC1 Activation and
755 Confers Resistance to PI3Kalpha Inhibition. Cancer cell 30:229-242.
756 Chalhoub N, Zhu G, Zhu X, Baker SJ (2009) Cell type specificity of PI3K signaling
757 in Pdk1- and Pten-deficient brains. Genes & development 23:1619-1624.
758 Chen XR, Heck N, Lohof AM, Rochefort C, Morel MP, Wehrle R, Doulazmi M,
759 Marty S, Cannaya V, Avci HX, Mariani J, Rondi-Reig L, Vodjdani G, Sherrard RM,
760 Sotelo C, Dusart I (2013) Mature Purkinje cells require the retinoic acid-related
761 orphan receptor-alpha (RORalpha) to maintain climbing fiber mono-innervation
762 and other adult characteristics. The Journal of neuroscience : the official journal of
763 the Society for Neuroscience 33:9546-9562.
764 Cordon-Barris L, Pascual-Guiral S, Yang S, Gimenez-Llort L, Lope-Piedrafita S,
765 Niemeyer C, Claro E, Lizcano JM, Bayascas JR (2016) Mutation of the
766 3-Phosphoinositide-Dependent Protein Kinase 1 (PDK1) Substrate-Docking Site in
767 the Developing Brain Causes Microcephaly with Abnormal Brain Morphogenesis
768 Independently of Akt, Leading to Impaired Cognition and Disruptive Behaviors.
769 Molecular and cellular biology 36:2967-2982.
770 Cupolillo D, Hoxha E, Faralli A, De Luca A, Rossi F, Tempia F, Carulli D (2016)
771 Autistic-Like Traits and Cerebellar Dysfunction in Purkinje Cell PTEN Knock-Out
772 Mice. Neuropsychopharmacology 41:1457-1466.
773 Dainichi T, Hayden MS, Park SG, Oh H, Seeley JJ, Grinberg-Bleyer Y, Beck KM,
774 Miyachi Y, Kabashima K, Hashimoto T, Ghosh S (2016) PDK1 Is a Regulator of
775 Epidermal Differentiation that Activates and Organizes Asymmetric Cell Division.
776 Cell reports 15:1615-1623.

777 Edamakanti CR, Do J, Didonna A, Martina M, Opal P (2018) Mutant ataxin1 disrupts
778 cerebellar development in spinocerebellar ataxia type 1. J Clin Invest
779 128:2252-2265.
780 Ferreira TA, Blackman AV, Oyrer J, Jayabal S, Chung AJ, Watt AJ, Sjostrom PJ, van
781 Meyel DJ (2014) Neuronal morphometry directly from bitmap images. Nat
782 Methods 11:982-984.
783 Gibson DA, Ma L (2011) Mosaic analysis of gene function in postnatal mouse brain
784 development by using virus-based Cre recombination. J Vis Exp.
785 Grego-Bessa J, Bloomekatz J, Castel P, Omelchenko T, Baselga J, Anderson KV
786 (2016) The tumor suppressor PTEN and the PDK1 kinase regulate formation of the
787 columnar neural epithelium. Elife 5:e12034.
788 Hirai H (2018) Protein Kinase C in the Cerebellum: Its Significance and Remaining
789 Conundrums. Cerebellum 17:23-27.
790 Itoh Y, Higuchi M, Oishi K, Kishi Y, Okazaki T, Sakai H, Miyata T, Nakajima K,
791 Gotoh Y (2016) PDK1-Akt pathway regulates radial neuronal migration and
792 microtubules in the developing mouse neocortex. Proceedings of the National
793 Academy of Sciences of the United States of America 113:E2955-2964.
794 Kano M, Hashimoto K, Chen C, Abeliovich A, Aiba A, Kurihara H, Watanabe M,
795 Inoue Y, Tonegawa S (1995) Impaired synapse elimination during cerebellar
796 development in PKC gamma mutant mice. Cell 83:1223-1231.
797 Lawlor MA, Mora A, Ashby PR, Williams MR, Murray-Tait V, Malone L, Prescott
798 AR, Lucocq JM, Alessi DR (2002) Essential role of PDK1 in regulating cell size
799 and development in mice. The EMBO journal 21:3728-3738.
800 Leroux AE, Schulze JO, Biondi RM (2018) AGC kinases, mechanisms of regulation
801 and innovative drug development. Semin Cancer Biol 48:1-17.
802 Liu C, Mei M, Li Q, Roboti P, Pang Q, Ying Z, Gao F, Lowe M, Bao S (2017) Loss of
803 the golgin GM130 causes Golgi disruption, Purkinje neuron loss, and ataxia in mice.
804 Proceedings of the National Academy of Sciences of the United States of America
805 114:346-351.
806 Liu R, Yang Y, Shen J, Chen H, Zhang Q, Ba R, Wei Y, Li KC, Zhang X, Zhao C

(2015) Fstl1 is involved in the regulation of radial glial scaffold development. Mol Brain 8:53.

Lui NC, Tam WY, Gao C, Huang JD, Wang CC, Jiang L, Yung WH, Kwan KM (2017) Lhx1/5 control dendritogenesis and spine morphogenesis of Purkinje cells via regulation of Espin. Nat Commun 8:15079.

Mucha BE et al. (2019) A new microdeletion syndrome involving TBC1D24, ATP6V0C, and PDPK1 causes epilepsy, microcephaly, and developmental delay. Genet Med 21:1058-1064.

Nakazono A, Adachi N, Takahashi H, Seki T, Hamada D, Ueyama T, Sakai N, Saito N (2018) Pharmacological induction of heat shock proteins ameliorates toxicity of mutant PKCgamma in spinocerebellar ataxia type 14. The Journal of biological chemistry 293:14758-14774.

Nam SM, Seo JS, Go TH, Nahm SS, Chang BJ (2019) Ascorbic Acid Supplementation Prevents the Detrimental Effects of Prenatal and Postnatal Lead Exposure on the Purkinje Cell and Related Proteins in the Cerebellum of Developing Rats. Biol Trace Elem Res 190:446-456.

Oishi K, Watatani K, Itoh Y, Okano H, Guillemot F, Nakajima K, Gotoh Y (2009) Selective induction of neocortical GABAergic neurons by the PDK1-Akt pathway through activation of Mash1. Proceedings of the National Academy of Sciences of the United States of America 106:13064-13069.

Peng N, Meng N, Wang S, Zhao F, Zhao J, Su L, Zhang S, Zhang Y, Zhao B, Miao J (2014) An activator of mTOR inhibits oxLDL-induced autophagy and apoptosis in vascular endothelial cells and restricts atherosclerosis in apolipoprotein E(-)/(-) mice. Sci Rep 4:5519.

Popa LS, Streng ML, Ebner TJ (2019) Purkinje Cell Representations of Behavior: Diary of a Busy Neuron. Neuroscientist 25:241-257.

Schrenk K, Kapfhammer JP, Metzger F (2002) Altered dendritic development of cerebellar Purkinje cells in slice cultures from protein kinase Cgamma-deficient mice. Neuroscience 110:675-689.

Shimobayashi E, Kapfhammer JP (2017) Increased biological activity of protein

Kinase C gamma is not required in Spinocerebellar ataxia 14. Mol Brain 10:34.

Srinivas S, Watanabe T, Lin CS, William CM, Tanabe Y, Jessell TM, Costantini F (2001) Cre reporter strains produced by targeted insertion of EYFP and ECFP into the ROSA26 locus. BMC Dev Biol 1:4.

Stanko JP, Easterling MR, Fenton SE (2015) Application of Sholl analysis to quantify changes in growth and development in rat mammary gland whole mounts. Reprod Toxicol 54:129-135.

Takahashi H, Adachi N, Shirafuji T, Danno S, Ueyama T, Vendruscolo M, Shuvaev AN, Sugimoto T, Seki T, Hamada D, Irie K, Hirai H, Sakai N, Saito N (2015) Identification and characterization of PKCgamma, a kinase associated with SCA14, as an amyloidogenic protein. Hum Mol Genet 24:525-539.

Takahashi N, Shuvaev AN, Konno A, Matsuzaki Y, Watanave M, Hirai H (2017) Regulatory connection between the expression level of classical protein kinase C and pruning of climbing fibers from cerebellar Purkinje cells. J Neurochem 143:660-670.

Takeo YH, Kakegawa W, Miura E, Yuzaki M (2015) RORalpha Regulates Multiple Aspects of Dendrite Development in Cerebellar Purkinje Cells In Vivo. The Journal of neuroscience : the official journal of the Society for Neuroscience 35:12518-12534.

Thomanetz V, Angliker N, Cloetta D, Lustenberger RM, Schweighauser M, Oliveri F, Suzuki N, Ruegg MA (2013) Ablation of the mTORC2 component rictor in brain or Purkinje cells affects size and neuron morphology. J Cell Biol 201:293-308.

Tolias KF, Bikoff JB, Burette A, Paradis S, Harrar D, Tavazoie S, Weinberg RJ, Greenberg ME (2005) The Rac1-GEF Tiam1 couples the NMDA receptor to the activity-dependent development of dendritic arbors and spines. Neuron 45:525-538.

Trzesniewski J, Altmann S, Jager L, Kapfhammer JP (2019) Reduced Purkinje cell size is compatible with near normal morphology and function of the cerebellar cortex in a mouse model of spinocerebellar ataxia. Exp Neurol 311:205-212.

Wang J, Liu Y, Chen T (2017a) Identification of key genes and pathways in Parkinson's disease through integrated analysis. Mol Med Rep 16:3769-3776.

867 Wang XQ, Lo CM, Chen L, Ngan ES, Xu A, Poon RY (2017b)
868 CDK1-PDK1-PI3K/Akt signaling pathway regulates embryonic and induced
869 pluripotency. Cell death and differentiation 24:38-48.
870 Wang Y, Chen ZP, Zhuang QX, Zhang XY, Li HZ, Wang JJ, Zhu JN (2017c) Role of
871 Corticotropin-Releasing Factor in Cerebellar Motor Control and Ataxia. Curr Biol
872 27:2661-2669 e2665.
873 Wong MMK, Hoekstra SD, Vowles J, Watson LM, Fuller G, Nemeth AH, Cowley SA,
874 Ansorge O, Talbot K, Becker EBE (2018) Neurodegeneration in SCA14 is
875 associated with increased PKCgamma kinase activity, mislocalization and
876 aggregation. Acta Neuropathol Commun 6:99.
877 Xenos D, Kamceva M, Tomasi S, Cardin JA, Schwartz ML, Vaccarino FM (2018)
878 Loss of TrkB Signaling in Parvalbumin-Expressing Basket Cells Results in
879 Network Activity Disruption and Abnormal Behavior. Cerebral Cortex
880 28:3399-3413.
881 Xu C, Yu L, Hou J, Jackson RJ, Wang H, Huang C, Liu T, Wang Q, Zou X, Morris
882 RG, Spires-Jones TL, Yang Z, Yin Z, Xu Y, Chen G (2017) Conditional Deletion of
883 PDK1 in the Forebrain Causes Neuron Loss and Increased Apoptosis during
884 Cortical Development. Front Cell Neurosci 11:330.
885 Xu M, Han X, Liu R, Li Y, Qi C, Yang Z, Zhao C, Gao J (2019) PDK1 Deficit Impairs
886 the Development of the Dentate Gyrus in Mice. Cereb Cortex 29:1185-1198.
887 Yoshida S, Sakagami H, Owada Y, Kokubun S, Kondo H (1999) Localization of
888 PDK-1 mRNA in the brain of developing and adult rats. The Tohoku journal of
889 experimental medicine 187:249-255.
890 Zurashvili T, Cordon-Barris L, Ruiz-Babot G, Zhou X, Lizcano JM, Gomez N,
891 Gimenez-Llort L, Bayascas JR (2013) Interaction of PDK1 with phosphoinositides
892 is essential for neuronal differentiation but dispensable for neuronal survival.
893 Molecular and cellular biology 33:1027-1040.

894

895 **Figure and Table legends**

896 **Figure 1. The distribution of PDK1-possitive cells in the cerebellum.** (A - D) $YFP^{+}$

cells are detected in the cerebellar PCs and interneurons in the *PV-cre*; *ROSA26-stop-EYFP* mice. (E - J'') Immunostaining for PDK1 at P14 (E - H) and P30 (I - J''). PDK1 is expressed in PCs (arrows in F, J and J'), the cells in the GCL (open arrowheads in F, J and J') and deep cerebellar nuclei (yellow arrowheads in H and J'') of the cerebellum. H is the boxed region in G. J, J' and J'' are the boxed regions in I which are labelled 1, 2, and 3, respectively. Scale bars: 100 μm for A - D, F, H and J - J''; 500 μm for E, G and I.

**Figure 2. The disruption of PDK1 in PCs and PV-positive cells in the ML of the cerebellum in the cKO-PV mice.** (A - F'') The expression of PDK1 is disrupted in PCs and PV-positive cells in the ML of cerebellum in the cKO-PV mice. Co-immunostaining for PDK1 (A, B, C, D, E and F) and GAD67 (A', B', C', D', E' and F') at P21 (A - B''), P40 (C - D'') and P60 (E - F''). In the Ctrl mice at P60, PDK1 is detected in PCs (arrows) and cells in the GCL (open arrowheads) and the ML (closed arrowheads) of cerebellum (E - E''), while in the cKO-PV mice, PDK1 is detected in cells in the GCL but not in PCs and cells in the ML of cerebellum (F - F''). (G) Western blotting for PDK1 from P60 cerebellar cortical lysates confirms the dramatic reduction of PDK1 protein level (left panel). The levels of PDK1 proteins were shown by the relative density normalized to GAPDH (right panel) and were analysed using a two-tailed Student's t-test. The data are the mean ± s.e.m.: 100.0 ± 13.23 in the Ctrl mice *vs* 37.29 ± 2.88 in the cKO-PV mice, n = 4 mice in each group, $p = 0.0320$ (* $p < 0.05$). Scale bars: 100 μm.

**Figure 3. Decreased cerebellar size in cKO-PV Mice.**

(A) Gross view of brains from the Ctrl and cKO-PV mice at P60. (B) Decreased cerebellar length and width in cKO-PV mice compared to those in Ctrl mice at P60. (C and D) Brain (C) and body (D) weights of the 9-week-old mice were not affected by the ablation of PDK1. (E - H') Immunostaining for calbindin at P14 (E and E'), P21 (F and F'), P60 (G and G') and P120 (H and H'). (I) The sagittal cross-sectional area of the cerebellar vermis. (J) The number of PCs per 100 μm length. (K - L) Total

number of PCs in the cerebellar Lobule V (K) and Lobule VI (L) at P60. The data are the mean ± s.e.m. Data in B - D were analysed using a two-tailed Student's t-test. A two-way ANOVA with Bonferroni's post hoc analysis was used in I - L. P-values: *** $p < 0.001$; ** $p < 0.01$; * $p < 0.05$; ns, $p \geq 0.05$; ### $p = 0.0003$. Scale bars: 5 mm for A; 500 μm for E - H'.

**Figure 4. The distribution and cytoarchitecture of cerebellar granule neurons and the morphology of Bergmann glial fibers in cKO-PV mice were comparable to those in Ctrl mice, but the ML thickness in lobule V was decreased after the ablation of PDK1.** (A - B'') The distribution and cytoarchitecture of cerebellar granule neurons in cKO-PV mice were comparable to those in Ctrl mice. Immunostaining for NeuN in Ctrl mice (A - A'') and cKO-PV mice (B - B'') at P21. (C - D'') The morphology of Bergmann glial fibers in cKO-PV mice were comparable to those in Ctrl mice. Immunostaining for GFAP in Ctrl mice (C - C'') and cKO-PV (D - D'') at P14. Scale bars: 1000 μm for A and B; 100 μm for A', A'', B', B'' and C - D''.

**Figure 5. Decrease of PCs cell body size, ML thickness and morphological complexity of dendrites in the cKO-PV Mice.**

(A - E') Immunostaining for calbindin at P14 (A and A'), P21 (B and B'), P30 (C and C'), P60 (D and D'), and P120 (E and E') indicated the decreased cell body size of PCs in cKO-PV mice. (F) Area of PCs cell body. (G - I') The ML was immunostained for calbindin at P30 (G and G'), P60 (H and H'), and P120 (I and I'). The straight line between the dotted line illustrates the thickness of the ML. (J and J') The ML thickness of the cerebellar Lobule V (J) and VI (J'). (K and K') Golgi staining of PCs in the Ctrl (K) and cKO-PV mice (K') at P30. (L) Sholl analysis: number of intersections of the dendrite at different distances from the cell body of PCs in the Ctrl and cKO-PV mice. A two-way ANOVA with respect to group effect; intersection number: $F(1, 2142) = 988.3$, $P < 0.001$; Bonferroni's *post hoc* comparison: * $p < 0.05$ between 45 mm and 65 mm from the cell body and *** $p < 0.001$ between 70 mm and 95 mm from the cell body. The data are the mean ± s.e.m. Statistical analysis used two-way ANOVA with

Bonferroni's *post hoc* analysis. P-values: *** $p < 0.001$; ** $p < 0.01$; * $p < 0.05$; ns, $p \geq 0.05$; ### $p < 0.001$ (P14 *vs* P21: $p < 0.0001$ in Lobule V and $p = 0.0001$ in Lobule VI). Scale bars: 50 μm for A to E', K and K'; 100 μm for G to I'.

**Figure 6. Motor Defects in cKO-PV mice.**

(A - A') Gait of 9 - 10 weeks old mice tested with a footprint assay was shown in red (fore paws) and blue (hind paws) (A and A'). (B) Diagram of parameters measured in footprint analysis. (C) The cKO-PV mice show similar stride length to the Ctrl mice. (D) The overlap length. (E - F) Longer sway lengths (E) and stance lengths (F) of forelimbs and hindlimbs in the cKO-PV mice. (G) Schematic illustration of the elevated beam-walk assay for testing motor coordination. (H) The latency to cross a 28 mm wide square beam at 8 weeks after birth. The Ctrl mice 9.46 ± 2.14 s ($n = 8$ mice) *vs* the cKO-PV mice 49.13 ± 10.87 s ($n = 4$ mice), $p = 0.0005$. (I) The average time 4-week-old mice took to traverse the round beams. (J) The average number of missteps for hindlimbs of 4-week old mice to traverse the round beams. (K) The latency to fall down from the rotarods in the cKO-PV mice ($n = 8$) was significantly reduced than that in the Ctrl mice ($n = 9$) at 4 weeks after birth. A two-way ANOVA; Bonferroni's post hoc analysis was used and P-values are: $p = 0.0055$ for 10 rpm test, $p < 0.0001$ for 15 rpm test, $p < 0.0001$ for 20 rpm test, $p < 0.0001$ for 25 rpm test, $p = 0.0154$ for 30 rpm test and $p = 0.3137$ for 33 rpm test. (L - O) Gait of 4-week old mice tested by footprint assay. Bar graphs show that there were no differences in the lengths of stride (L), overlap (M), stance (N), and sway (O) between the Ctrl and cKO-PV mice at 4 weeks. The data are the mean ± s.e.m. Data in C - F, H and L - O were analysed using a two-tailed Student's *t*-test and a two-way ANOVA; Bonferroni's *post hoc* analysis was used in I - K. P-values: *** $p < 0.001$; ** $p < 0.01$; * $p < 0.05$; ns, $p \geq 0.05$. Scale bar: 20 mm.

**Figure 7. PDK1 disruption in PCs of cKO-Pcp2 mice at P30.**

(A - B'') Co-immunostaining for PDK1 (A, B, A'' and B'') and GAD67 (A', B', A'' and B'') in cKO-Pcp2 mice (B - B'') and Ctrl mice (A - A'') at P30.

**Figure 8. Purkinje cell-specific ablation of PDK1 lead to decreased cell body size, ML thickness and motor defects in mice.**

(A -- B’’’) Immunostaining for calbindin at P30 in Ctrl and cKO-Pcp2 mice. Decreased cell body size of PDK1-deficient PCs in the cerebellar Lobule II-III (A’ and B’), Lobule V-VI (A’’ and B’’) and Lobule IX-X (A’’’ and B’’’). (C and D) Immunostaining for PDK1 at P30. (E) Decreased cell body area of PDK1-deficient PCs at P30. (F) The number of PCs per 100 μm at P30. (G) Decreased cerebellar size in cKO-Pcp2 mice at P30. (H) The ML thickness of Lobules V and VI at P30. (I) Latency to traverse the round beams. (J) The number of missteps. (K) Rotarod assay showed a defect motor coordination in cKO-Pcp2 mice at 9-week old. The number of mice used in this experiment are n = 9 mice for the Ctrl and n = 8 for the cKO-Pcp2 mice. A two-way ANOVA; Bonferroni’s *post hoc* analysis was used and P-values are: $p > 0.9999$ for 10 rpm test, $p > 0.9999$ for 15 rpm test, $p = 0.0421$ for 20 rpm test, $p < 0.0001$ for 25 rpm and 30 rpm test, and $p = 0.0065$ for 35 rpm test. The data are the mean ± s.e.m. Data in G and H were analysed using a two-tailed Student’s *t*-test and a two-way ANOVA; Bonferroni's *post hoc* analysis was used to analyse data in E, F and I - K. P-values: *** $p < 0.001$; ** $p < 0.01$; * $p < 0.05$; ns, $p \geq 0.05$. Scale bars: 1 mm for A and B; 100 μm for A’ to A’’’ and B’ to B’’’; 50 μm for C and D.

**Figure 9. Defects in spontaneous firing activity of PDK1-KO PCs.**

The electrophysiological characteristic of PCs was evaluated at P21. (A) Representative traces of 1.5 s duration from the control PCs (upper panel in A) and the PDK1-KOs PCs (lower panel in A). (B) The interspike-interval histogram of the PCs. (C) The spontaneous firing frequencies of PCs. Control PCs: 54.78 ± 7.82 Hz (n = 10 PCs from 6 mice) *vs* PDK1-KO PCs: 31.07 ± 4.50 Hz (n = 8 PCs from 6 mice), $p = 0.0259$. (D) Coefficients of variation (CV) of spontaneous firing of PCs. Control PCs: 0.11 ± 0.01 (n = 10 PCs from 6 mice) *vs* PDK1-KO PCs: 0.13 ± 0.04 (n = 8 PCs from 6 mice), $p = 0.5343$. (E) The membrane capacitance (Cm) of PCs. Control PCs: 720.10 ± 81.52 pf (n = 10 PCs from 6 mice) *vs* PDK1-KO PCs: 291.60 ± 46.35 pf (n

= 8 PCs from 6 mice), p = 0.0006. (F - H) The spontaneous EPSC of PDK1-KO PCs showed no difference compared to control PCs. (F) Representative traces 1.5 s sEPSC duration from the control PCs (upper panel in F) and the PDK1-KO PCs (lower panel in F). (G) The amplitudes of PCs sEPSC. Control PCs: 11.85 ± 1.03 pA (n = 5 PCs from 3 mice) *vs* PDK1-KO PCs: 11.21 ± 0.98 pA (n = 5 PCs from 3 mice), p = 0.6649. (H) The frequencies of sEPSC. Control PCs: 1.16 ± 0.25 Hz (n = 5 PCs from 3 mice) *vs* PDK1-KO PCs: 1.42 ± 0.33 Hz (n = 5 PCs from 3 mice), p = 0.5434. The data are the mean ± s.e.m. Data were analysed using a two-tailed Student's *t*-test. P-values: *** $p < 0.001$; * $p < 0.05$; ns: $p \geq 0.05$.

**Figure 10. Decreased phosphorylation level of ribosomal protein S6 and the decreased PCs body size was rescued by 3BDO in the cKO-PV mice.**

(A - D'') Co-immunostaining for pS6 (A, B, C, and D) and GAD67 (A', B', C', and D') at P14 (A - B'') and P21 (C - D''). (E - H) Co-immunostaining for pS6 (E, F, G, and H) and GAD67 (E', F', G', and H') at P30. Arrows indicate the PCs and arrowheads indicate the Bergmann glia in the cerebellum. (I - L) Immunostaining for calbindin at P30. (M) Area of PCs cell body in mice at P30. The data are the mean ± s.e.m.: 323.70 ± 3.57 $\mu m^2$ for vehicle-treated Ctrl mice (n = 149 PCs from 3 mice); 333.40 ± 8.24 $\mu m^2$ for 3BDO-treated Ctrl mice (n = 159 PCs from 3 mice); 213.04 ± 4.68 $\mu m^2$ for vehicle-treated cKO-PV mice (n = 85 PCs from 2 mice); and 254.00 ± 4.45 $\mu m^2$ for 3BDO-treated cKO-PV mice (n = 144 PCs from 3 mice). The P-value: Vehicle/Ctrl mice *vs* 3BDO/Ctrl mice: no significance; Vehicle/Ctrl mice *vs* Vehicle/cKO-PV mice: $p < 0.0001$; Vehicle/cKO-PV mice *vs* 3BDO/cKO-PV mice: p = 0.0137. (N) In the low rotational speed (15 and 20rpm), 3BDO treatment rescued the motor coordination in the cKO-PV mice. P-values of 3BDO treatment cKO-PV mice compared with vehicle treatment Ctrl mice: 10 rpm: $p > 0.999$, 15 rpm: p = 0.1228, 20 rpm: p = 0.2065, 25 rpm: p = 0.0047 and 30 and 33 rpm: $p < 0.0001$. The number of the mice used in the experiments were n = 12 for the vehicle-treated Ctrl mice group and n = 7 for the 3BDO-treated cKO-PV mice group. The data are the mean ± s.e.m. A two-way ANOVA; Bonferroni's *post hoc* analysis was used to analyse

data in M and N. P-values: *** $p < 0.001$, ** $p < 0.01$ and ns, $p \geq 0.05$. Scale bars: 100 μm for A to H; 50 μm for I to L.

**Figure 11. Decreased expression levels of PKCγ in cKO-PV mice and rescue of deficient dendritic complexity by overexpressing PKCγ.**

(A - C') Immunostaining for pPKCγ at P21 (A and A'), at P30 (B and B') and at P40 (C and C') shows progressive loss of staining intensity in cKO-PV mice. (D - E'') pPKCγ was totally disrupted in the PCs after the ablation of PDK1 at P60. pPKCγ: green and GAD67: red. Scale bars: 100 μm. (F) Representative blots with the antibody of PKCγ. (F') Quantification of PKCγ levels in the cerebellum lysates from Ctrl and cKO-PV mice at P21. Amount of PKCγ was normalized to β-actin. The value obtained in Ctrl mice were set to 100. The data are the mean ± s.e.m.: Ctrl: 100.0 ± 2.9, n = 4 mice; cKO-PV: 66.0 ± 9.3, n = 4 mice, $p = 0.0131$. (G) Representative blots with the antibody of calbindin. (G') Quantification of calbindin levels. Ctrl: 100.0 ± 2.1, n = 4 mice; cKO-PV: 111.6 ± 25.0, n = 4 mice, $p = 0.6609$. Data in F' and G' were analysed using a two-tailed Student's *t*-test. P-values: * $p < 0.05$ and ns, $p \geq 0.05$.

**Figure 12. The rescue of deficient dendritic complexity by overexpressing PKCγ in the PDK1-KO PCs from the PDK1 cKO-Pcp2 mice.**

(A and B) Immunostaining for mCherry shows the rAAV-mCherry infected PCs in lobule IV (A) and lobule IX (B) in Ctrl mice. (C - F) Immunostaining for GFP shows the rAAV-EGFP infected PCs (C and D) and the rAAV-pPKCγ overexpressing PCs (E and F) in lobule IV (C and E) and lobule IX (D and F) in cKO-Pcp2 mice. (G and H) The schematic illustration of the Sholl analysis of rAAV infected PCs. 20 mm radius steps are shown in the illustration. AAV2/9-CAG-FLEX -EGFP infected PCs in cKO-Pcp2 mice (G) and AAV2/9-CAG-FLEX-Prkcg-3xHA-P2A-EGFP infected PCs in cKO-Pcp2 mice (H). (I) Sholl analysis for three groups of PCs in panel G - L at P30. The red curve represented the rAAV-mCherry infected PCs in Ctrl mice (n = 18 PCs from 5 mice). The green curve represented the rAAV-EGFP infected PCs (n = 21 PCs

from 3 mice) and the blue curve represented the PCs overexpressing pPKCγ (n = 43 PCs from 3 mice) in cKO-Pcp2 mice. The number of intersections of the dendrite at different distances from the cell body of PCs and the data are the mean ± s.e.m.. A two-way ANOVA; Bonferroni's *post hoc* analysis was used: rAAV-mCherry/Ctrl mice *vs* rAAV-EGFP/cKO-Pcp2 mice, *** P < 0.001 between 50 mm and 135 mm from the cell body. rAAV-EGFP/cKO-Pcp2 mice *vs* rAAV-PKCγ/cKO-Pcp2 mice: ## P < 0.01 between 55 mm and 75 mm from the cell body and # P < 0.05 between 80 mm and 110 mm from the cell body. (J) The cumulative length of the dendritic arbour of PCs. The data are the mean ± s.e.m.: rAAV-mCherry/Ctrl mice: 6.31 ± 0.20 mm, n = 18 PCs from 5 mice; rAAV-EGFP/cKO-Pcp2 mice: 3.45 ± 0.35 mm, n = 21 PCs from 3 mice (p < 0.0001, compared to that in rAAV-mCherry/Ctrl mice); and rAAV-PKCγ/cKO-Pcp2 mice: 4.55 ± 0.12 mm, n = 43 PCs from 3 mice (p = 0.0007, compared to that in rAAV-EGFP/cKO-Pcp2). (K) Dendritic tree area of PCs. The data are the mean ± s.e.m.: rAAV-mCherry/Ctrl mice: 16.59 ± 0.65 $\times 10^3$ $\mu m^2$, n = 18 PCs form 5 mice; rAAV-EGFP/cKO-Pcp2 mice: 12.19 ± 0.96 $\times 10^3$ $\mu m^2$, n = 21 PCs form 3 mice (p = 0.0001, compared to that in rAAV-mCherry/Ctrl mice); and rAAV-PKCγ/cKO-Pcp2 mice: 14.26 ± 0.42 $\times 10^3$ $\mu m^2$, n = 43 PCs form 3 mice (p = 0.0392, compared to that in rAAV-EGFP/cKO-Pcp2 mice). Data in I were analysed using a two-way ANOVA; Bonferroni's *post hoc* analysis and a one-way ANOVA; Bonferroni's *post hoc* analysis was used to analyse data in J and K. P-values: ### p < 0.001, ## p < 0.01, # p < 0.05, *** p < 0.001. Scale bars: 100 μm.

**Table 1: The statistical data of brain morphology in the cKO-PV and Ctrl mice.** The data are the mean ± s.e.m. P-values: * p < 0.05; ns, p ≥ 0.05.

**Table 2: The statistical data for morphological analysis of the cerebellum in the cKO-PV and Ctrl mice.** The data are the mean ± s.e.m. P-values: *** p < 0.001; ** p < 0.01; * p < 0.05; ns, p ≥ 0.05.

**Table 3: The statistical data for footprint tests in the cKO-PV and Ctrl mice at 4**

**and 8 - 9 weeks after birth.** The data are the mean ± s.e.m. P-values: *** $p < 0.001$; ** $p < 0.01$; * $p < 0.05$; ns, $p \geq 0.05$.

**Table 4: The statistical data for elevated beam-walk in the 4-week old cKO-PV and Ctrl mice.** The data are the mean ± s.e.m. P-values: *** $p < 0.001$; * $p < 0.05$; ns, $p \geq 0.05$.

**Table 5: The statistical data for morphological analysis of the cerebellum in the cKO-Pcp2 and Ctrl mice at P30.** The data are the mean ± s.e.m. P-values: *** $p < 0.001$; * $p < 0.05$; ns, $p \geq 0.05$.

**Table 6: The statistical data for elevated beam-walk in the 9-week old cKO-Pcp2 and Ctrl mice.** The data are the mean ± s.e.m. P-values: *** $p < 0.001$; ** $p < 0.01$; ns, $p \geq 0.05$.

**Movies**

**Movie 1. *Pdk1*$^{fl/fl}$ mouse at P36.**

**Movie 2. *PV-cre*; *Pdk1*$^{fl/fl}$ mouse at P36.**

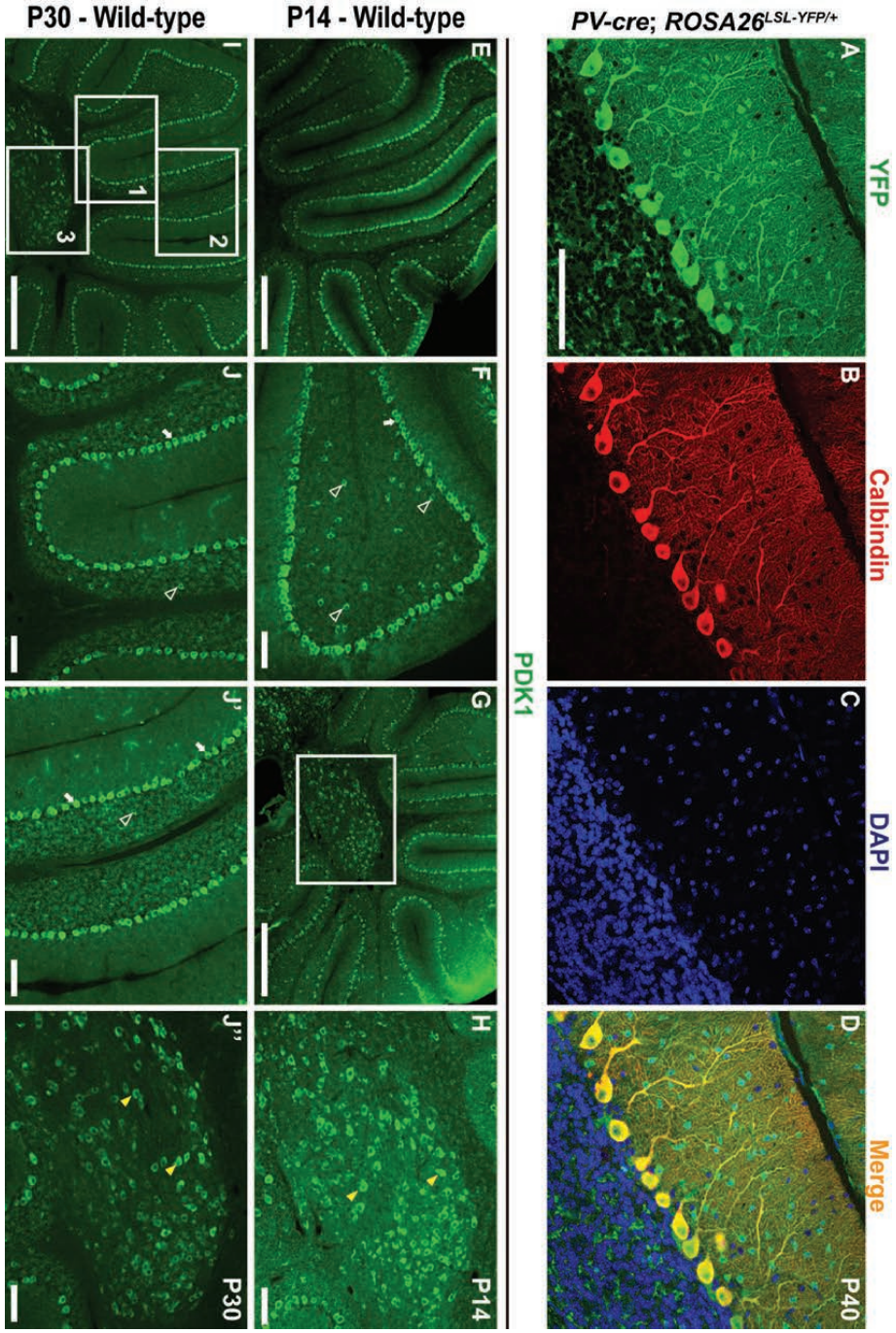

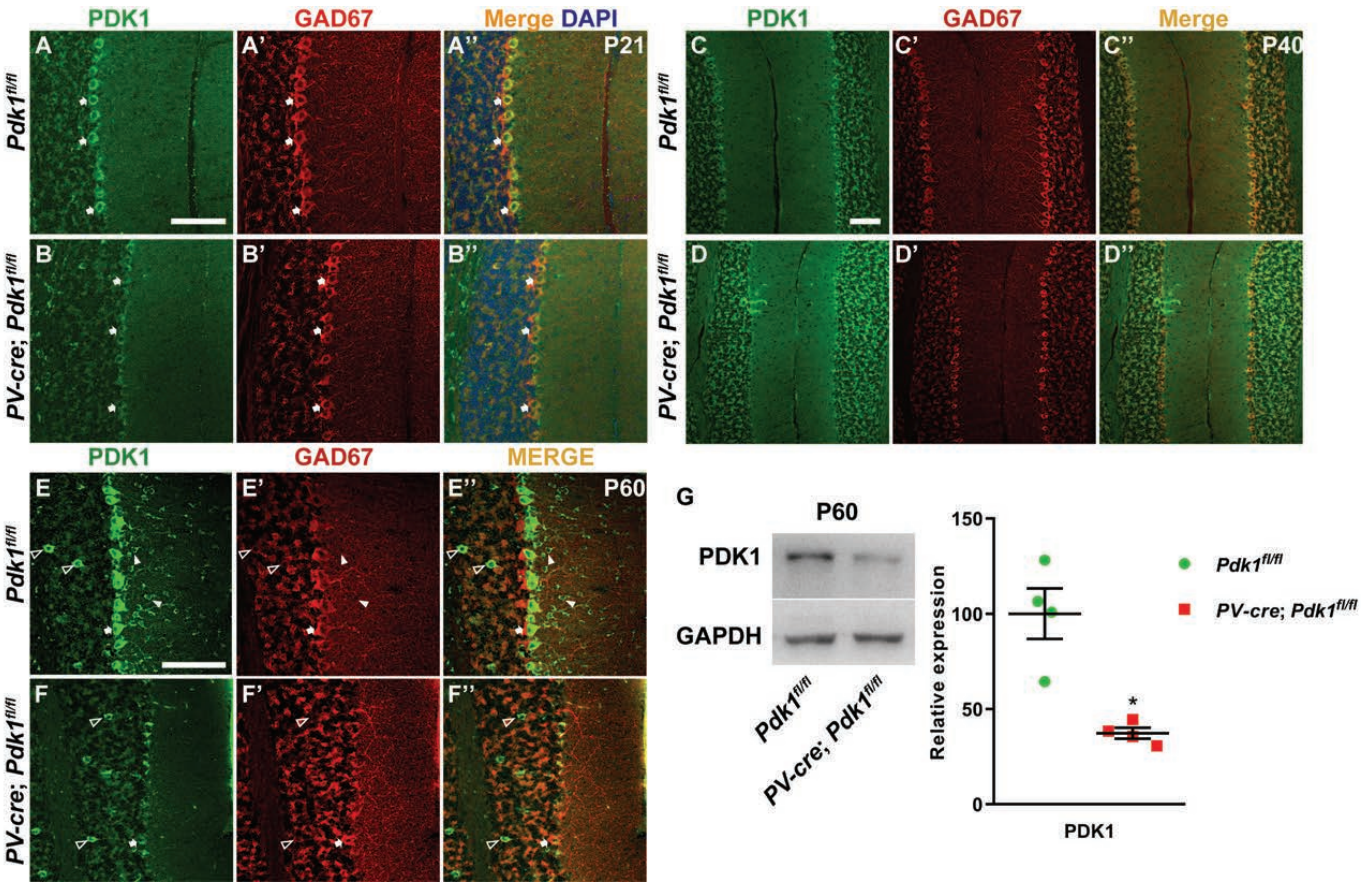

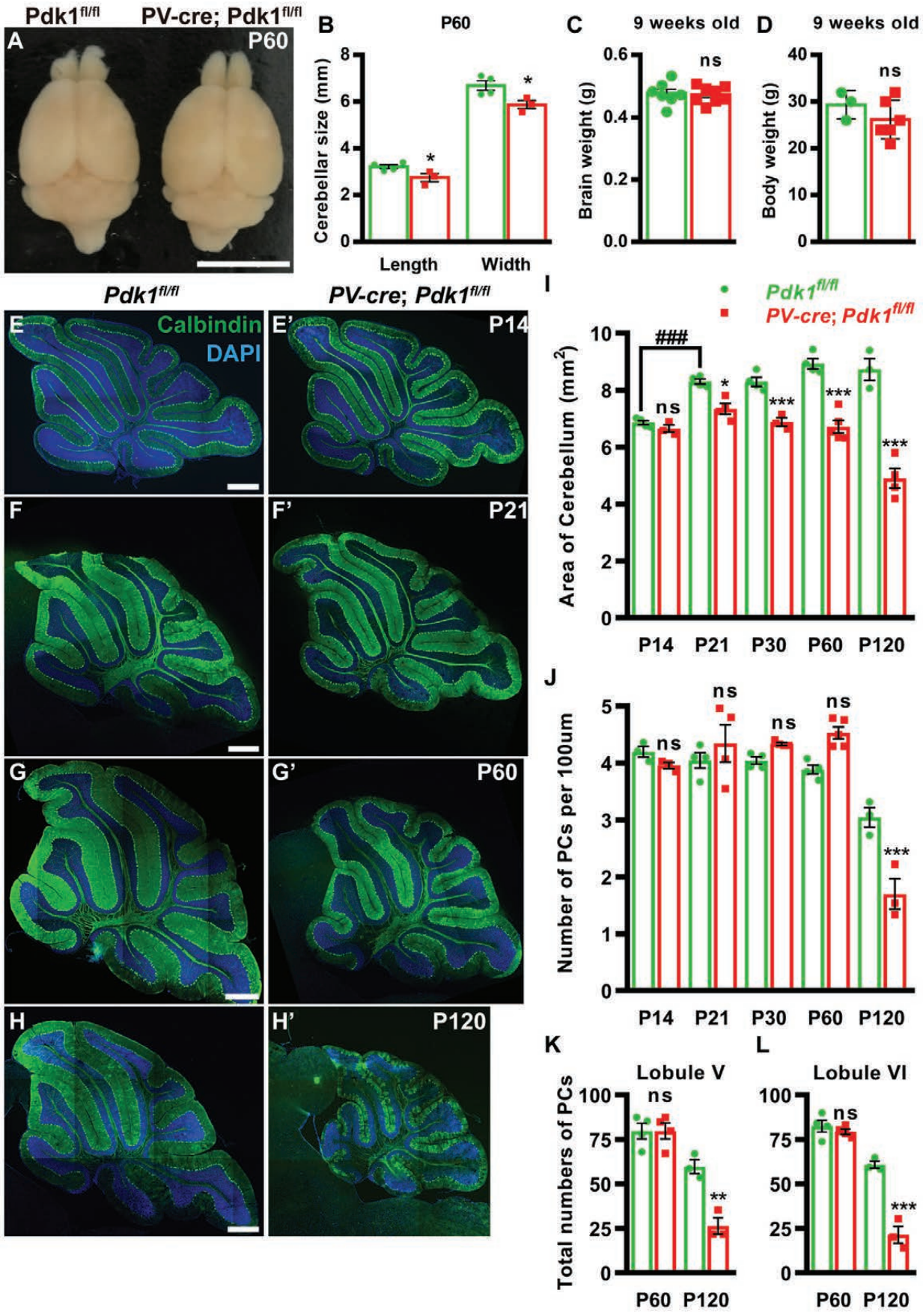

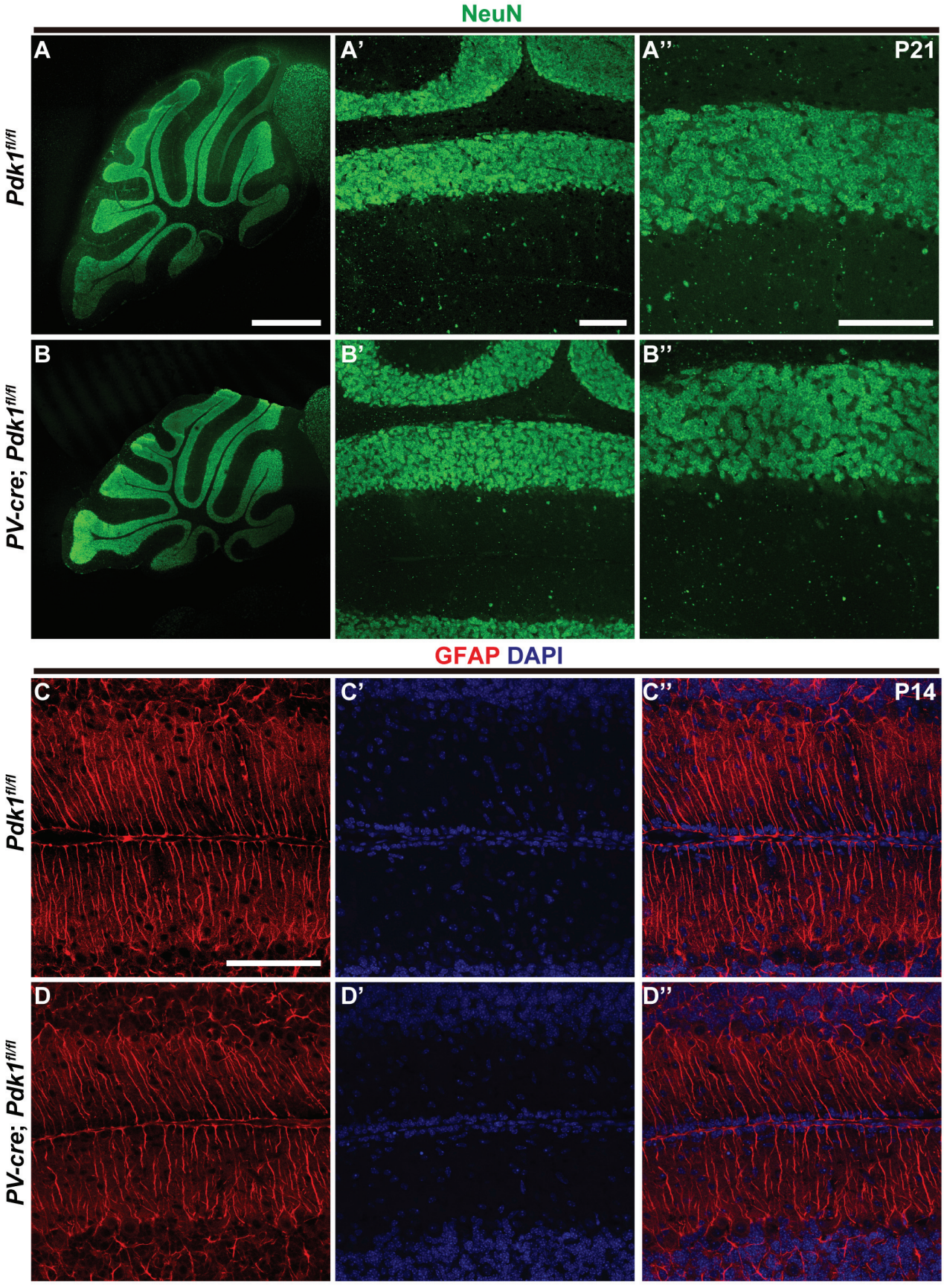

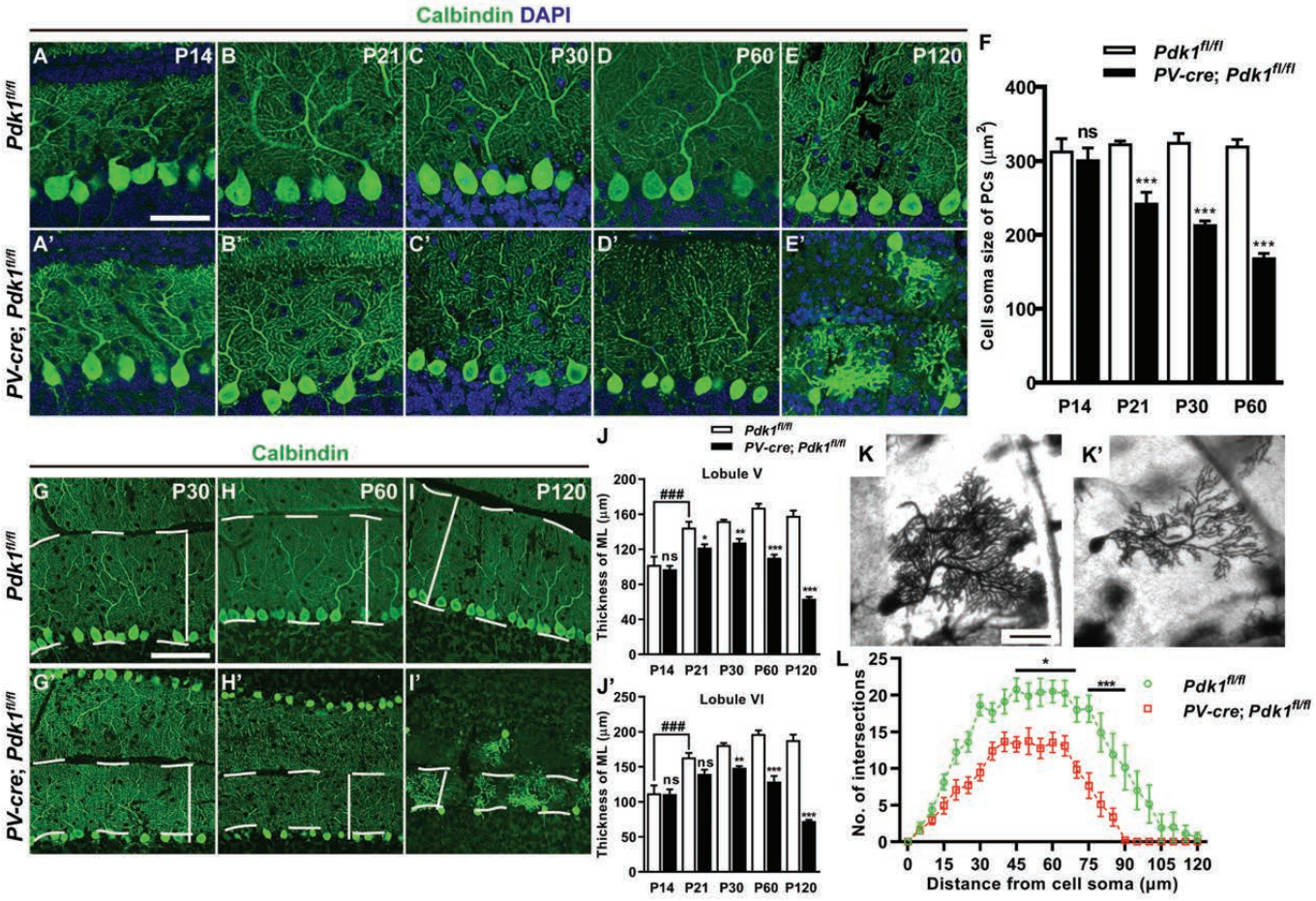

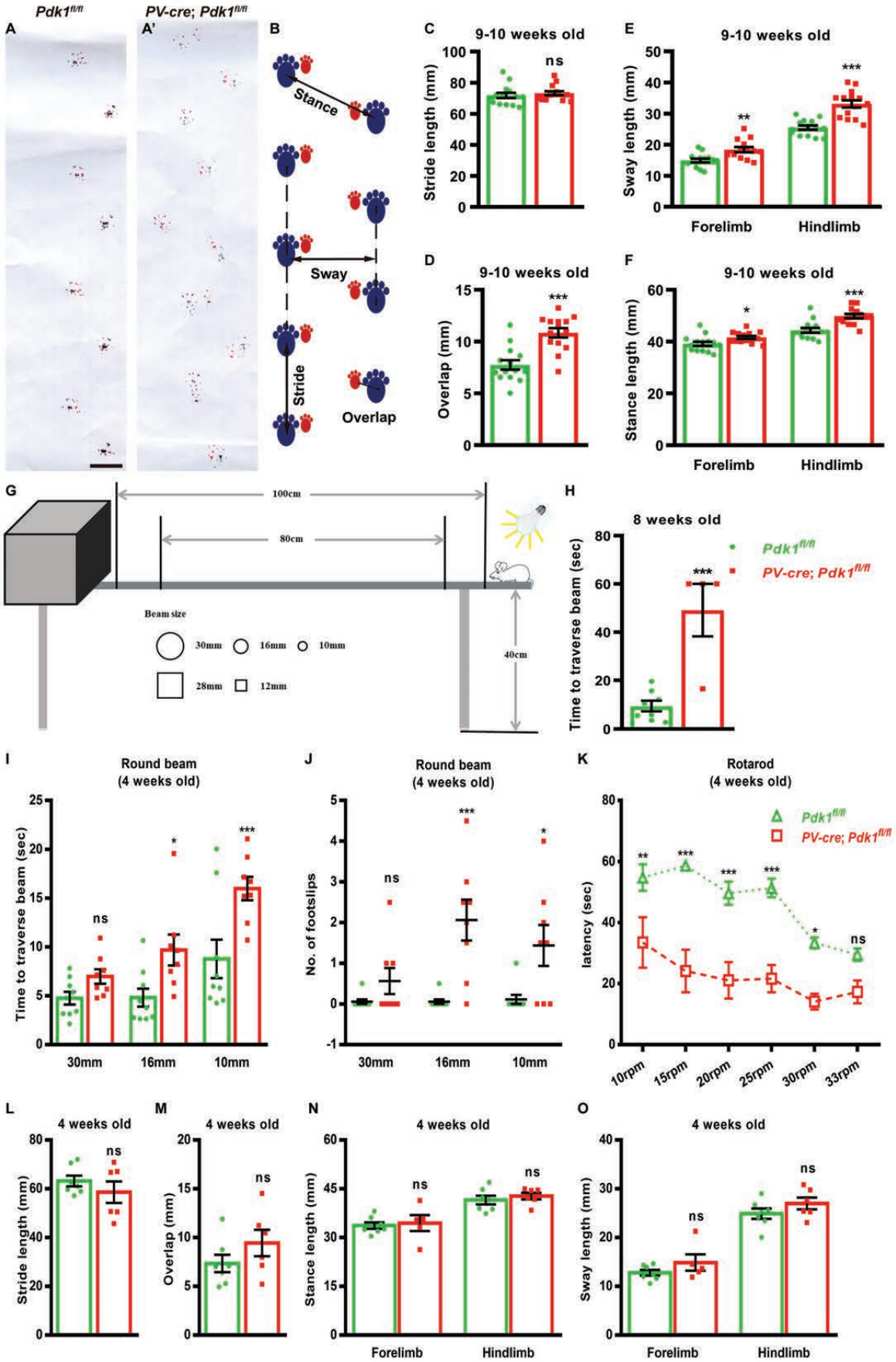

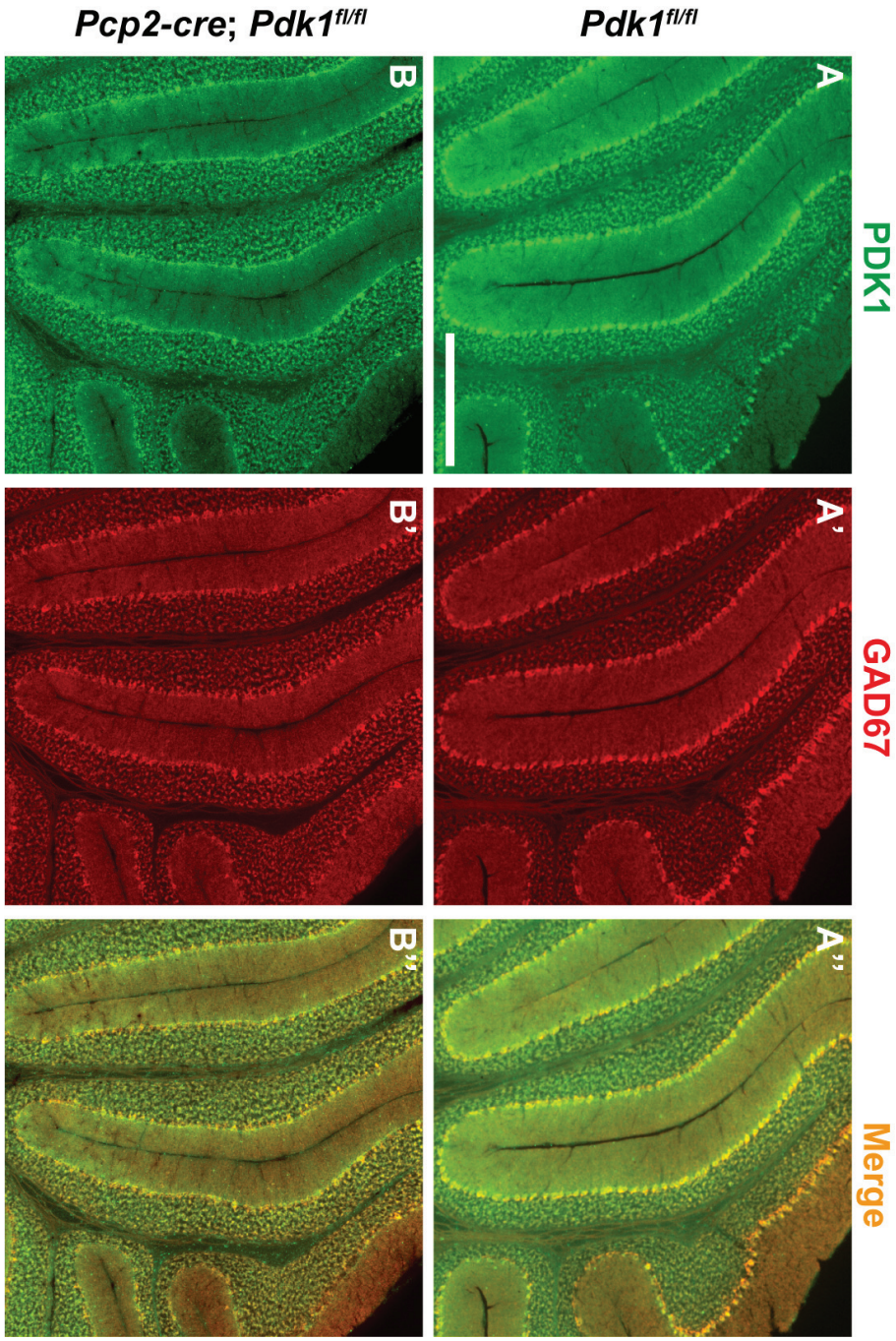

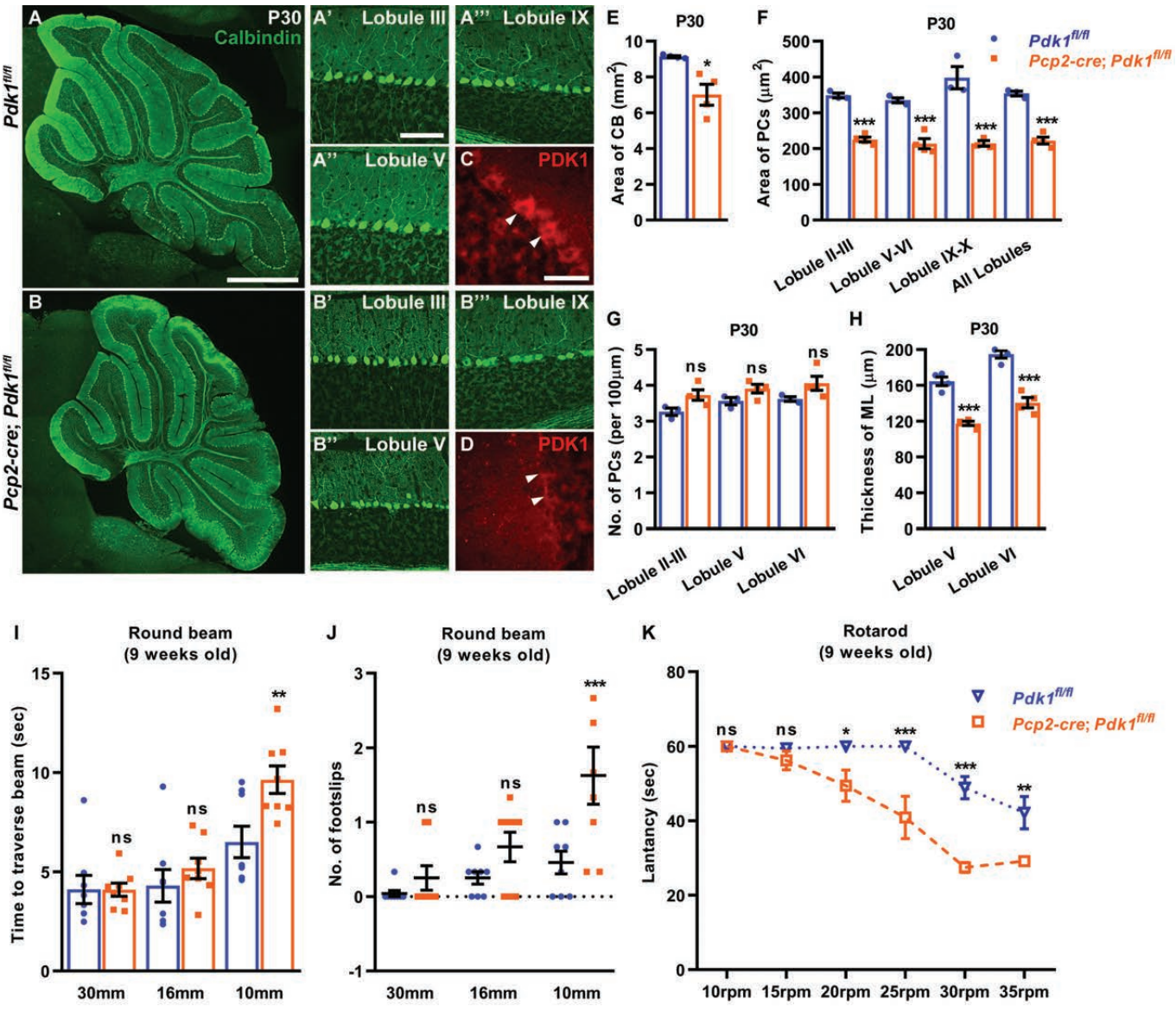

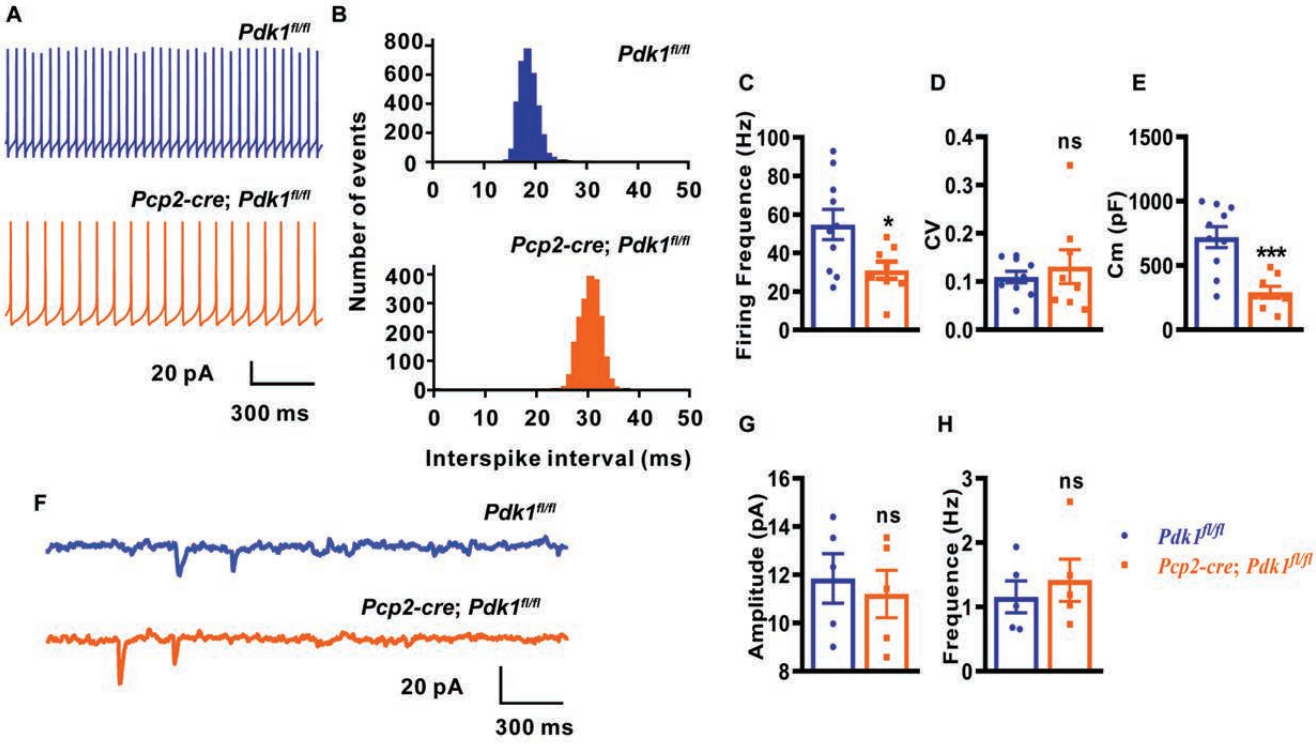

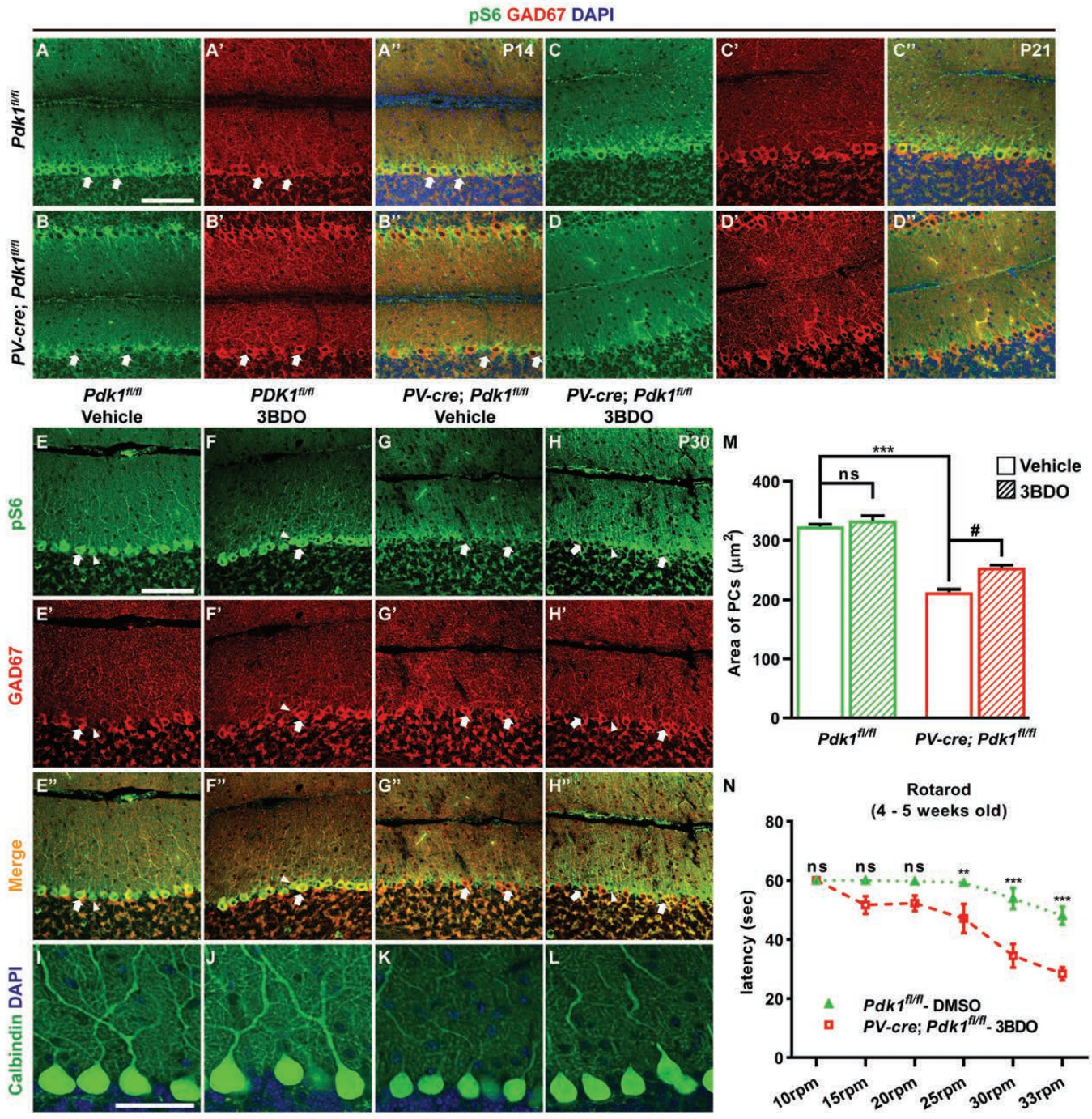

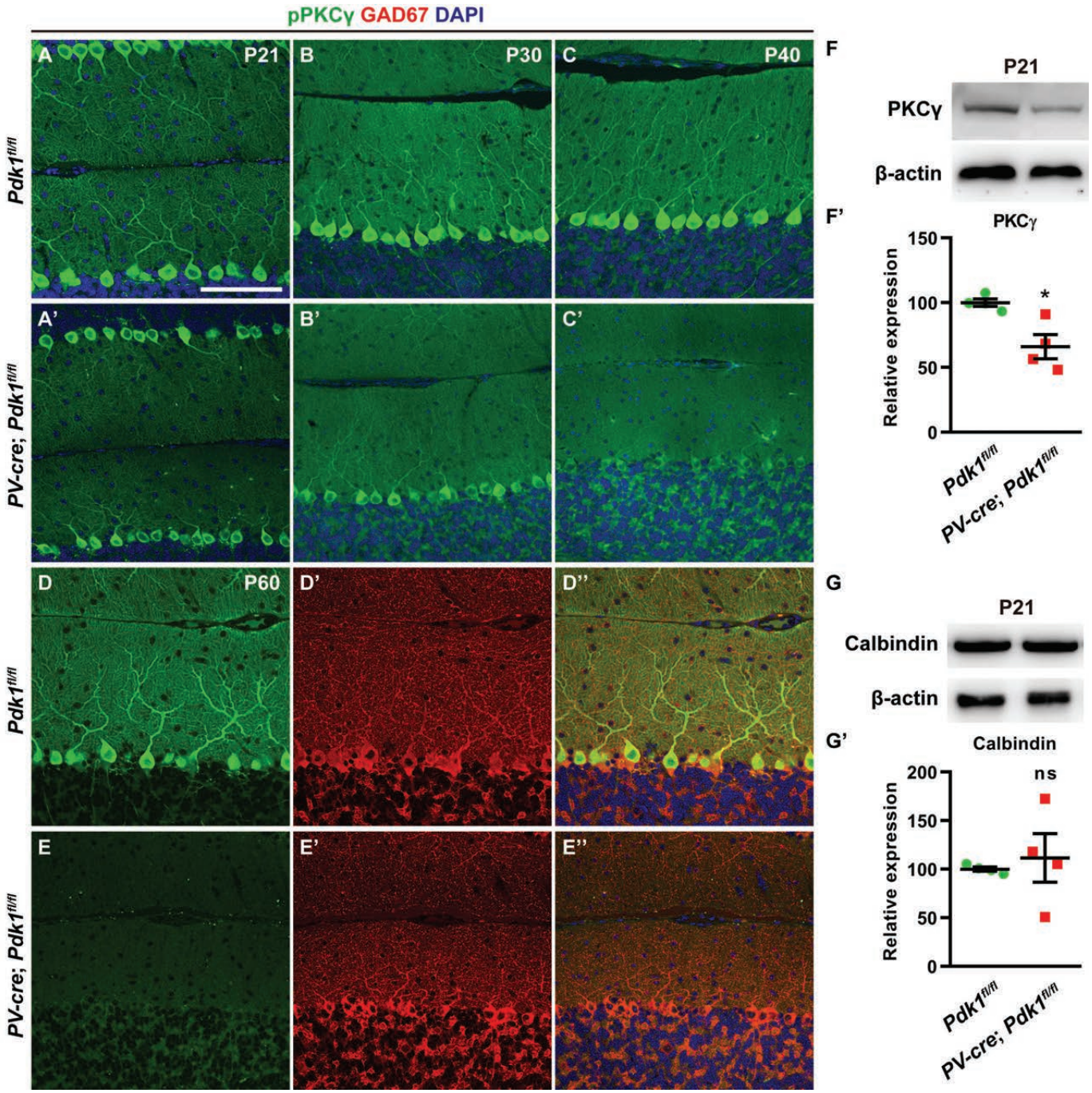

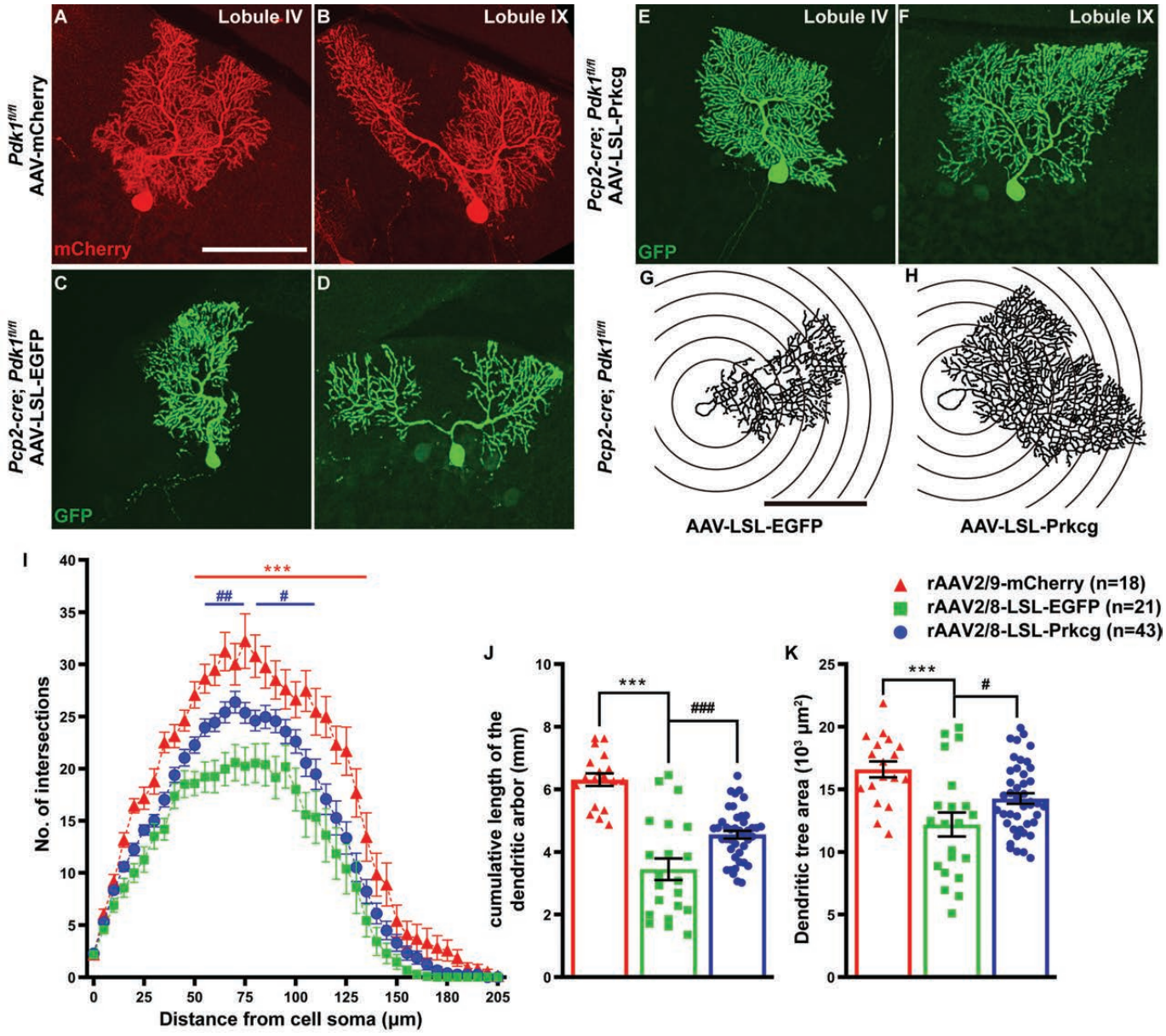

**Table 1: The statistical data of brain morphology in the cKO-PV and Ctrl mice.**

| | Ctrl | cKO-PV | p-value |
|---|---|---|---|
| The cerebellar length (mm) | 3.22 ± 0.08 (n = 4) | 2.75 ± 0.17 (n = 3) * | 0.0425 |
| The cerebellar width (mm) | 6.70 ± 0.20 (n = 4) | 5.87 ± 0.18 (n = 3) * | 0.0324 |
| Brain weight (g) | 0.48 ± 0.01 (n = 7) | 0.47 ± 0.01 (n = 8) ns | 0.8031 |
| Body weight (g) | 29.33 ± 1.76 (n = 3) | 26.17 ± 1.68 (n = 6) ns | 0.2823 |

The data are the mean ± s.e.m. P-values: * $p < 0.05$; ns, $p \geq 0.05$.

**Table 2: The statistical data for morphological analysis of the cerebellum in the cKO-PV and Ctrl mice.**

| | Age | P14 | P21 | P30 | P60 | P120 |
|---|---|---|---|---|---|---|
| The area of cerebellar middle sagittal sections ($mm^2$) | Ctrl | 6.86 ± 0.07 (n = 4) | 8.30 ± 0.09 (n = 4) | 8.30 ± 0.16 (n = 4) | 8.94 ± 0.18 (n = 4) | 8.73 ± 0.39 (n = 3) |
| | cKO-PV | 6.64 ± 0.13 (n = 3) $^{ns}$ | 7.35 ± 0.19 (n = 4) $^{*}$ | 6.88 ± 0.15 (n = 3) $^{***}$ | 6.72 ± 0.22 (n = 5) $^{***}$ | 4.90 ± 0.34 (n = 4) $^{***}$ |
| | p-value | > 0.9999 | 0.0140 | 0.0005 | < 0.0001 | < 0.0001 |
| The number of PCs per 100 μm length | Ctrl | 4.20 ± 0.10 (n = 3) | 4.05 ± 0.14 (n = 4) | 4.04 ± 0.06 (n = 4) | 3.89 ± 0.08 (n = 4) | 3.05 ± 0.17 (n = 3) |
| | cKO-PV | 3.96 ± 0.05 (n = 3) $^{ns}$ | 4.35 ± 0.33 (n = 4) $^{ns}$ | 4.34 ± 0.02 (n = 4) $^{ns}$ | 4.53 ± 0.11 (n = 5) $^{ns}$ | 1.70 ± 0.27 (n = 3) $^{***}$ |
| | p-value | > 0.9999 | > 0.9999 | > 0.9999 | 0.1903 | 0.0005 |
| Total number of PCs in cerebellar Lobule V | Ctrl | | | | 79.74 ± 4.41 (n = 4) | 59.75 ± 3.89 (n = 3) |
| | cKO-PV | | | | 79.80 ± 4.51 (n = 4) $^{ns}$ | 26.30 ± 4.56 (n = 3) $^{**}$ |
| | p-value | | | | > 0.9999 | 0.0012 |
| Total number of PCs in cerebellar Lobule VI | Ctrl | | | | 82.61 ± 3.32 (n = 4) | 60.83 ± 2.00 (n = 3) |
| | cKO-PV | | | | 79.47 ± 1.55 (n = 4) $^{ns}$ | 21.50 ± 4.73 (n = 3) $^{***}$ |

| | | | | | | |
|---|---|---|---|---|---|---|
| | p-value | | | | 0.8988 | < 0.0001 |
| Area of PCs cell body ($\mu m^2$) | Ctrl | 314.21 ± 15.79 (n = 4) | 323.85 ± 3.26 (n = 4) | 325.91 ± 11.21 (n = 4) | 321.06 ± 8.07 (n = 4) | |
| | cKO-PV | 302.29 ± 15.10 (n = 3)$^{ns}$ | 243.71 ± 13.88 (n = 4)$^{***}$ | 214.40 ± 4.47 (n = 4)$^{***}$ | 169.46 ± 5.33 (n = 5)$^{***}$ | |
| | p-value | > 0.9999 | < 0.0001 | < 0.0001 | < 0.0001 | |
| The ML thickness of the cerebellar Lobule V (μm) | Ctrl | 102.20 ± 9.43 (n = 4) | 144.73 ± 6.50 (n = 3) | 152.23 ± 1.58 (n = 4) | 167.49 ± 4.30 (n = 4) | 158.08 ± 5.96 (n = 3) |
| | cKO-PV | 97.10 ± 3.99 (n = 3)$^{ns}$ | 121.94 ± 3.82 (n = 4)$^{*}$ | 127.71 ± 4.27 (n = 4)$^{**}$ | 110.24 ± 3.66 (n = 4)$^{***}$ | 63.59 ± 2.05 (n = 3)$^{***}$ |
| | p-value | > 0.9999 | 0.0250 | 0.0072 | < 0.0001 | < 0.0001 |
| The ML thickness of the cerebellar Lobule VI (μm) | Ctrl | 112.27 ± 11.13 (n = 4) | 163.44 ± 6.37 (n = 3) | 181.08 ± 2.63 (n = 4) | 196.98 ± 5.18 (n = 4) | 188.18 ± 7.71 (n = 3) |
| | cKO-PV | 111.21 ± 6.58 (n = 3)$^{ns}$ | 139.97 ± 5.76 (n = 4)$^{ns}$ | 148.58 ± 2.36 (n = 4)$^{**}$ | 128.78 ± 8.21 (n = 4)$^{***}$ | 72.72 ± 1.51 (n = 3)$^{***}$ |
| | p-value | > 0.9999 | 0.1030 | 0.0053 | < 0.0001 | < 0.0001 |

The data are the mean ± s.e.m. P-values: *** $p < 0.001$; ** $p < 0.01$; * $p < 0.05$; ns, $p \geq 0.05$.

**Table 3: The statistical data for footprint tests in the cKO-PV and Ctrl mice at 4 and 8 - 9 weeks after birth.**

| | Age | 4-week old | 8~9-week old |
|---|---|---|---|
| The stride distance | Ctrl | 63.17 ± 2.21 (n = 7) | 71.82 ± 1.75 (n = 14) |
| | cKO-PV | 58.61 ± 4.41 (n = 6) $^{ns}$ | 73.23 ± 1.31 (n = 14) $^{ns}$ |
| | p-value | 0.3543 | 0.5239 |
| The overlap distance (mm) | Ctrl | 7.34 ± 0.90 (n = 7) | 7.75 ± 0.45 (n = 14) |
| | cKO-PV | 9.44 ± 1.360 (n = 6) $^{ns}$ | 10.85 ± 0.45 (n = 14) $^{***}$ |
| | p-value | 0.2126 | < 0.0001 |
| The sway distance of fore limbs (mm) | Ctrl | 12.78 ± 0.58 (n = 7) | 14.93 ± 0.60 (n = 14) |
| | cKO-PV | 14.87 ± 1.66 (n = 5) $^{ns}$ | 18.39 ± 0.82 (n = 14) $^{**}$ |
| | p-value | 0.2064 | 0.0020 |
| The sway distance of hind limbs (mm) | Ctrl | 24.88 ± 1.05 (n = 7) | 25.49 ± 0.69 (n = 14) |
| | cKO-PV | 26.98 ± 1.20 (n = 6) $^{ns}$ | 33.13 ± 1.17 (n = 14) $^{***}$ |
| | p-value | 0.2145 | < 0.0001 |
| The stance lengths of fore limbs (mm) | Ctrl | 33.70 ± 1.00 (n = 7) | 39.16 ± 0.83 (n = 14) |
| | cKO-PV | 34.43 ± 2.46 (n = 5) $^{ns}$ | 41.64 ± 0.56 (n = 14) $^{*}$ |
| | p-value | 0.7622 | 0.0205 |
| The stance lengths of hind limbs (mm) | Ctrl | 41.55 ± 1.32 (n = 7) | 44.38 ± 0.93 (n = 14) |
| | cKO-PV | 42.74 ± 1.02 (n = 6) $^{ns}$ | 49.85 ± 0.84 (n = 14) $^{***}$ |
| | p-value | 0.5013 | 0.0002 |

The data are the mean ± s.e.m. P-values: *** $p < 0.001$; ** $p < 0.01$; * $p < 0.05$; ns, $p \geq 0.05$.

**Table 4: The statistical data for elevated beam-walk in the 4-week old cKO-PV and Ctrl mice.**

| | The diameter of the round beam | 30 mm | 16 mm | 10 mm |
|---|---|---|---|---|
| Time to traverse beam (sec) | Ctrl | 4.75 ± 0.65 (n = 9) | 4.81 ± 0.92 (n = 9) | 8.76 ± 1.97 (n = 9) |
| | cKO-PV | 6.97 ± 0.74 (n = 8) $^{ns}$ | 9.68 ± 1.59 (n = 8) $^{*}$ | 15.98 ± 1.19 (n = 8) $^{***}$ |
| | p-value | 0.6812 | 0.0293 | 0.0007 |
| Nombers of footslips | Ctrl | 0.06 ± 0.06 (n = 9) | 0.06 ± 0.06 (n = 9) | 0.11 ± 0.11 (n = 9) |
| | cKO-PV | 0.56 ± 0.32 (n = 8) $^{ns}$ | 2.06 ± 0.50 (n = 8) $^{***}$ | 1.44 ± 0.50 (n = 8) $^{*}$ |
| | p-value | 0.7388 | <0.0001 | 0.0108 |

The data are the mean ± s.e.m. P-values: *** $p < 0.001$; * $p < 0.05$; ns, $p \geq 0.05$.

**Table 5: The statistical data for morphological analysis of the cerebellum in the cKO-Pcp2 and Ctrl mice at P30.**

| | Ctrl | cKO-Pcp2 | p-value |
|---|---|---|---|
| The area of cerebellar middle sagittal sections ($mm^2$) | 9.14 ± 0.05 (n = 4) | 7.01 ± 0.58 (n = 4) * | 0.0104 |
| Area of PCs cell body in the Lovbule II-III ($\mu m^2$) | 348.31 ± 6.53 (n = 3) | 225.19 ± 6.74 (n = 4) *** | < 0.0001 |
| Area of PCs cell body in the Lovbule V-VI ($\mu m^2$) | 334.75 ± 6.96 (n = 3) | 213.67 ± 13.98 (n = 4) *** | < 0.0001 |
| Area of PCs cell body in the Lovbule IX-X ($\mu m^2$) | 398.02 ± 30.87 (n = 3) | 214.25 ± 7.88 (n = 3) *** | < 0.0001 |
| Average area of PCs cell body in the CB ($\mu m^2$) | 353.87 ± 6.81 (n = 3) | 222.33 ± 9.34 (n = 4) *** | < 0.0001 |
| The number of PCs per 100μm length in the Lovbule II-III | 3.26 ± 0.10 (n = 3) | 3.73 ± 0.14 (n = 4) ns | 0.1091 |
| The number of PCs per 100μm length in the Lovbule V | 3.56 ± 0.10 (n = 3) | 3.91 ± 0.12 (n = 4) ns | 0.3177 |
| The number of PCs per 100μm length in the Lovbule VI | 3.62 ± 0.06 (n = 3) | 4.06 ± 0.20 (n = 4) ns | 0.1405 |
| The ML thickness of the cerebellar Lobule V (μm) | 164.56 ± 4.86 (n = 4) | 117.45 ± 2.37 (n = 4) *** | < 0.0001 |

| | | | |
|---|---|---|---|
| The ML thickness of the cerebellar Lobule VI (μm) | 194.81 ± 4.16 (n = 4) | 140.65 ± 5.84 (n = 4) *** | < 0.0001 |

The data are the mean ± s.e.m. P-values: *** $p < 0.001$; * $p < 0.05$; ns, $P \geq 0.05$.

**Table 6: The statistical data for elevated beam-walk in the 9-week old cKO-Pcp2 and Ctrl mice.**

| | The diameter of the round beam | 30 mm | 16 mm | 10 mm |
|---|---|---|---|---|
| Time to traverse beam (sec) | Ctrl | 4.11 ± 0.71 (n = 8) | 4.29 ± 0.81 (n = 8) | 6.50 ± 0.79 (n = |
| | cKO-Pcp2 | 4.10 ± 0.33 (n = 8) $^{ns}$ | 5.18 ± 0.51 (n = 8) $^{ns}$ | 9.64 ± 0.69 (n = 8) $^{**}$ |
| | p-value | >0.9999 | >0.9999 | 0.0053 |
| Nombers of footslips | Ctrl | 0.04 ± 0.04 (n = 8) | 0.25 ± 0.08 (n = 8) | 0.46 ± 0.15 (n = 8) |
| | cKO-Pcp2 | 0.25 ± 0.16 (n = 8) $^{ns}$ | 0.67 ± 0.20 (n = 8) $^{ns}$ | 1.62 ± 0.3 (n = 8) $^{***}$ |
| | p-value | >0.9999 | 0.4624 | 0.0006 |

The data are the mean ± s.e.m. P-values: *** $p < 0.001$; ** $p < 0.01$; ns, $p \geq 0.05$.